RETROSPECTIVE RADIATION DOSIMETRY USING OPTICALLY STIMULATED LUMINESCENCE OF ELECTRONIC COMPONENTS

DOSIMÉTRIE RETROSPECTIVE PAR LUMINESCENCE STIMULÉE OPTIQUEMENT DE COMPOSANTS DE DISPOSITIFS ÉLECTRONIQUES

A Thesis Submitted

to the Division of Graduate Studies of the Royal Military College of Canada

by

Elizabeth Lynne Inrig

In Partial Fulfillment of the Requirements for the Degree of

Master of Applied Science

October 2009

Your file Votre référence
ISBN: 978-0-494-57735-6
Our file Notre référence
ISBN: 978-0-494-57735-6

ACKNOWLEDGEMENTS

Completion of this thesis would not have been possible without the assistance of many individuals. First and foremost, I would like to thank my supervisors, Dr. Bill Andrews and Dr. Kathy Creber, for their guidance, advice, and patience.

I would also like to thank my colleagues at Defence Research and Development Canada, particularly Dr. Dorothy Godfrey-Smith, who introduced me to the field of luminescence research and collaborated on several of the experiments presented in this thesis. I also owe a great deal to my Group Leader, Dr. Lorne Erhardt, and my former Group Leader, Dr. Tom Cousins, for their flexibility and understanding while I attempted to balance both work and academic commitments.

Finally, I would like to thank my parents, Scott and Christine Inrig, and my grandmother, Jean Holliday, for their love and support during the writing process and throughout my academic career.

ABSTRACT

Inrig, Elizabeth Lynne; MASc (Nuclear Engineering); Royal Military College of Canada; October 2009; Retrospective Radiation Dosimetry Using Optically Stimulated Luminescence of Electronic Components; Dr. W.S. Andrews and Dr. K. Creber.

This work investigated the feasibility of using materials from personal electronic devices for optically stimulated luminescence (OSL) based retrospective dosimetry following a radiological accident or attack. The alumina porcelain substrates of surface-mount resistors were identified as the most sensitive and ubiquitous components for OSL analysis. Studies were conducted on resistor samples and cellular phone components in order to characterise the dose response and signal stability of the substrates. Anomalous signal fading was observed, and procedures were developed to correct for this. Dose reconstruction procedures were validated through trials in which cellular phones were affixed to an anthropomorphic phantom, irradiated with a gamma source, and analysed following delays of 4 to 21 days. Doses from 0.1-0.6 Gy were successfully reconstructed using the single aliquot regenerative-dose (SAR) protocol, incorporating a fading correction. It was concluded that resistors from cellular phones and other portable electronic devices should be considered for use as retrospective dosimeters in the case of unforeseen radiation exposures.

Keywords: aluminum oxide, anomalous fading, ceramics, electronics, OSL, luminescence, resistors, retrospective dosimetry.

RÉSUMÉ

Inrig, Elizabeth Lynne; MASc (génie nucléaire); Collège militaire royal du Canada; octobre 2009; Dosimétrie de rayonnement rétrospective au moyen de la luminescence stimulée optiquement de composants électroniques; Dr W.S. Andrews et Dr. K. Creber.

Pour le présent travail, on a étudié la possibilité d'utiliser des matériaux provenant de dispositifs électroniques personnels pour de la dosimétrie rétrospective basée sur la luminescence stimulée optiquement (LSO), suite à un accident ou une attaque radiologique. On a déterminé que les substrats en porcelaine et alumine de résistances montées en surface sont les éléments les plus sensibles et les plus répandus pour une analyse par LSO. On a réalisé des études sur des échantillons de résistance et des éléments de téléphone portables afin de caractériser la dose réponse et la stabilité du signal de ces substrats. On a observé que le signal analogue s'estompait, et on a développé des procédures pour y remédier. Les procédures de reconstruction de la dose ont été validées au moyen d'essais au cours desquels des téléphones portables ont été fixés sur un fantôme anthropomorphique irradié par une source gamma, puis analysés après un délai de 4 à 21 jours. Des doses de 0,1-0,6 Gy ont pu être reconstruites au moyen du protocole de dose régénérative d'aliquote simple, tenant compte d'un facteur de correction pour l'estompage. On a conclu que l'utilisation comme dosimètre rétrospectif de résistances de téléphones portables et d'autres dispositifs électroniques devrait être envisagée dans le cas d'expositions imprévues à du rayonnement.

Mots clés : oxyde d'aluminium, estompage anormal, céramique, électronique, LSO, luminescence, résistances, dosimétrie rétrospective.

TABLE OF CONTENTS

LIST OF TABLES

LIST OF FIGURES

LIST OF ABBREVIATIONS

a.u.	arbitrary units
cps	counts per second
CW-OSL	Continuous wave optically stimulated luminescence
D_e	Equivalent dose
DRDC	Defence Research and Development Canada
ED	Electronic dosimeter
EPR	Electron paramagnetic resonance
FOM	Figure of merit
IR-OSL	Infrared optically stimulated luminescence
LED	Light emitting diode
LM-OSL	Linearly modulated optically stimulated luminescence
OSL	Optically stimulated luminescence
PMT	Photomultiplier tube
RDD	Radiological dispersal device
RED	Radiological exposure device
SAR	Single aliquot regenerated-dose
TL	Thermoluminescence

CHAPTER 1: INTRODUCTION

For more than forty years, radiation doses to exposed populations in contaminated areas have been estimated by using luminescence techniques to analyse bricks and other radiation-sensitive building materials and household objects. More recently, researchers have begun to consider the problem of individual dose reconstruction using personal effects, such as electronic components from cellular phones and telephone chip-cards (Inrig *et al.*, 2008, Göksu *et al.*, 2003). Applications to forensics, where the dose imparted to building materials and household chemicals is used to identify former storage locations of radiological materials, have also been explored (Larsson *et al.*, 2005). In the current security climate, there is an increased awareness of the potential threat posed by terrorist groups, should they acquire radiological materials for use in an attack on a civilian target. Although there is an entire industry devoted to the protection and monitoring of radiation workers, it is clear that in the event of a radiological accident or attack involving exposure to the general public, the vast majority of those exposed will not be equipped with radiation dosimeters of any kind.

According to the U.S. Department of Homeland Security's Emergency Radiation Dose Assessment Program's technology assessment, there is currently no method that is capable of rapidly detecting whole body doses of 1-8 Gy within the first 72 hours of exposure (U.S. Department of Homeland Security, 2005). This is the gap that this work proposes to address. In the aftermath of a widespread exposure to radiation, such as might occur following the detonation of a radiological dispersal device (RDD) or even the deployment of a radiological exposure device (RED), health care professionals will be quickly overwhelmed. The task of carrying out triage to distinguish between the potentially exposed and the worried-well is time-

consuming, and current biological dosimetry methods are generally unable to provide results in less than a week. While cytogenetic chromosome aberration assessment has been used to estimate doses as low as 0.2 Gy by scoring 1000 metaphase spreads, cytogenetic triage (with 40-50 metaphase spreads) is ineffective below 1 Gy (U.S. Department of Homeland Security, 2005).

A rapid method of assessing external radiation exposure using commonly-held personal objects (essentially "fortuitous" dosimeters) would thus be invaluable for triage purposes. This approach has already garnered international attention. Several research groups have begun to investigate the optically stimulated luminescence (OSL) and thermoluminescence (TL) properties of electronic components (Beerten *et al.*, 2009, Woda, 2009); indeed, the use of electronic components in retrospective dosimetry was reported in a recent review article covering developments in OSL materials and techniques for dosimetry (Pradhan, 2008). In addition, the NATO Defence Against Terrorism (DAT) program has funded a project, led by Canada, to develop a portable OSL instrument capable of analyzing electronic components and other materials in the field, in order to arrive at rapid dose estimates for triage.The provision of timely individual dose estimates through OSL analysis of personal items is both desirable and achievable. Ideally, a "fortuitous dosimeter" should be positioned close to the body, be carried by a large percentage of the population, and be sufficiently sensitive to detect doses below the threshold for deterministic health effects. This threshold may vary from person to person, and while whole-body exposures of less than 1 Gy often product no symptoms, the IAEA (1998) defines a dose $\geq$ 0.25 Sv as a significant whole-body exposure. Since analysis would most likely be performed close to the time of exposure (within days to months), the measured dose response from the material of interest need not be completely stable so long as procedures can be developed to correct for signal fading. This research aims to demonstrate that, in principle,

cellular phones and other electronic devices fulfill all of these requirements, and can be used successfully for individual dose reconstruction.

CHAPTER 2: LUMINESCENCE TECHNIQUES FOR RETROSPECTIVE DOSIMETRY

2.1 Introduction and background

When certain insulating materials are exposed to ionizing radiation, they store some of the absorbed or deposited energy in the form of metastable excited molecular states. In some cases, luminescence is emitted when light is used to stimulate the release of this stored energy. This process is known as optically stimulated luminescence (OSL), and its application to passive radiation dosimetry is at the foundation of this thesis. OSL is the optical analogue of a somewhat more well-known and better-established process, thermoluminescence (TL), where the release of stored energy is stimulated by the application of heat. For both OSL and TL, the intensity of the emitted luminescence is proportional to the radiation dose imparted to the material; thus, both are effective tools for radiation dosimetry (Bøtter-Jensen *et al.*, 2003b).

While optically stimulated luminescence is a relatively recent discovery, thermoluminescence was first reported in 1663, when Robert Boyle presented his observations of the luminescence emitted by a diamond upon exposure to body heat. In her doctoral thesis (1903), Marie Curie described the thermoluminescence of calcium fluoride following exposure to radium, and commented that once the material had been heated and luminescence had been observed, it was necessary to expose the material to radium again before the observation could be repeated. The development of materials for TL dosimetry began in the 1940s, where lithium fluoride emerged as the most suitable TL material; LiF is the major constituent of TLD 100, still one of the most widely-used TL phosphors (McKinlay, 1981).

Compared to TL, techniques and technologies based on OSL have only recently emerged. Although OSL was first suggested for dosimetry by Antonov-Romanovskii *et al.* (1955), and again by others at the First International Conference on Luminescence Dosimetry (Bräunlich *et al.*, 1965, Sanborn and Beard, 1965), it did not gain widespread use. McKeever (2002) suggests that this was mainly due to the lack of a suitable OSL material that exhibited high sensitivity to radiation, low effective atomic number, and high signal stability at ambient temperatures. OSL came into widespread use for geological and archaeological dating following the publication of work by Huntley *et al.* (1985). This was followed by the demonstration by Godfrey-Smith and Haskell (1993) of the potential for the use of quartz OSL in retrospective accident dosimetry. It has, in fact, been widely used to estimate population doses in areas where there has been widespread contamination and exposure, such as the Chernobyl exclusion zone (Bailiff, 1995). OSL finally emerged as a practical tool for personal dosimetry and medical dosimetry in the mid-1990s, with the advent of methods involving pulsed OSL (POSL) of Al_2O_3:C (McKeever *et al.*, 1996a).

In the last ten years, the possibility of using OSL dosimetry to determine radiation doses to individuals, as opposed to populations, has garnered a great deal of attention. Recent studies have proposed the use of telephone chip-cards (Göksu, 2003, Göksu and Bailiff, 2006) and ID card memory chip modules (Mathur *et al.*, 2007) for dose reconstruction, and preliminary results suggest that these may be suitable for evaluating doses in the 1-10 Gy range relevant for triage (Mathur *et al.*, 2007). Substrates and semiconductor components of electronic devices are beginning to be explored for dosimetry; monocrystalline silicon carbide (SiC), also known as moissanite or carborundum, is found in certain high-frequency devices, and has recently been used to detect doses as low as 0.7 Gy (Godfrey-Smith, 2006). Some of the early results of the

work presented here were published in the proceedings of the 15th International Conference on Solid-State Dosimetry (SSD-15), and other groups have since begun to publish similar results (Inrig *et al.*, 2008, Beerten *et al.*, 2009, Woda, 2009).

This chapter will discuss the principles of retrospective dosimetry and describe the use of OSL in dose reconstruction. It will also review some concepts that are relevant to this work, including luminescence theory, dose estimation procedures, and instrumentation.

2.2 Retrospective dosimetry

Luminescence-based retrospective dosimetry has two primary applications: retrospective accident dosimetry, and luminescence dating, used in geology and archaeology. The IAEA defines a radiation accident as "an unintended or unexpected event occurring with a radiation source, or during a practice involving ionising radiation, which may result in significant human exposure and/or material damage" (IAEA, 1998). Retrospective accident dosimetry aims to provide a quantitative assessment of the radiation dose to individuals, and to the population as a whole, following such an exposure. The exposure in question may be due to an accident, such as the one that occurred at the Chernobyl nuclear power plant in the Ukraine, or an attack by terrorists or a hostile state in the form of a radiological dispersal device (RDD), radiological exposure device (RED), or even a nuclear weapon. The process of dose estimation following such an event is known as dose reconstruction, and serves to inform medical practitioners on the best course of treatment for exposed individuals, as well as to provide data for long-term epidemiological studies relating cancer rates to radiation exposure (Aitken, 1998, Bøtter-Jensen *et al.*, 2003b). Because luminescence dosimetry methods allow for the measurement of the cumulative absorbed dose, they are particularly useful for dose reconstruction. Many materials have highly stable luminescence signals and can be analyzed several years after an event,

ensuring that dose estimates are available regardless of whether or not radiation monitoring equipment was in use in the area at the time of exposure (Bøtter-Jensen *et al.*, 2003b). Previously, a limitation of luminescence-based techniques has been that while methods such as electron spin resonance (ESR) of tooth enamel have permitted the measurement of radiation doses to individuals, luminescence techniques have only been able to provide information on doses to populations (Aitken, 1998). The techniques described in this thesis will attempt to address this gap to some degree.

2.2.1 Geological and archaeological dating

The first widespread application of optically stimulated luminescence was in the area of geological dating, as first suggested by Huntley, Godfrey-Smith, and Thewalt in their article, "Optical dating of sediments," published in *Nature* in 1985. Their study was motivated by a desire to improve on the thermoluminescence dating methods in use at the time (Aitken, 1998). They proposed that by measuring the OSL signal from a mineral sample and determining the environmental dose rate resulting from the decay of naturally-occurring radioisotopes, the time since the sediment had last been exposed to light could be calculated, thus determining the sediment's date of deposition. Their first experiments examined two sets of samples, covering the age ranges of 0-700 ka and 0-6 ka, for which independent age information was available. A 514.5 nm argon-ion laser was used for stimulation of α-quartz extracted from the sediments, and the observed OSL signal showed the expected age-dependence. A second series of experiments compared the equivalent doses obtained using the new OSL method to those determined using the "partial-bleach" TL method, with good agreement for 5 and 60 ka samples (Huntley *et al.*, 1985).

Quartz and feldspar are the minerals most commonly used in optical dating, but others, such as volcanic glass and zircon, have also been used. Aeolian, or wind-borne, sediments are generally preferred for dating, as grains are likely to be well-bleached by exposure to sunlight before deposition, ensuring zeroing of the luminescence signal. In archaeological dating using pottery and burnt stones, the initial zeroing of the OSL signal is provided by heat (Aitken, 1998).

Samples are separated by mineral composition and particle size, and measurements are generally made on notionally equivalent portions of the separated material, known as aliquots. The initial, or "natural", luminescence signal from the sample is measured and compared to the signals generated by known doses administered in the laboratory; the laboratory dose required to produce a signal equivalent to the initial luminescence of the sample is referred to as the paleodose. Figure 1 illustrates the accumulation of the luminescence signal following the most recent bleaching event (Aitken, 1998).

The age of the sample is then obtained by dividing the paleodose by the dose rate, where the dose rate is evaluated through on-site and in-laboratory measurement of the radioactivity of the sediment (Aitken, 1998). A number of different procedures can be used for evaluation of the paleodose, including multiple- and single-aliquot additive and regenerative methods.

The natural OSL signal arises mainly from exposure to potassium (^{40}K) and isotopes in the thorium and uranium decay chains. Additional minor contributions come from cosmic rays and rubidium. At sea level, the cosmic-ray dose rate is roughly 0.18 Gy/ka at a depth of 1 metre, with an additional 14% attenuation per metre in rock or sediment having a density of approximately 2 g/cm^3. The effect of cosmic radiation becomes significant at high altitudes, and is largely due to the more penetrating component of cosmic radiation, particularly muons and

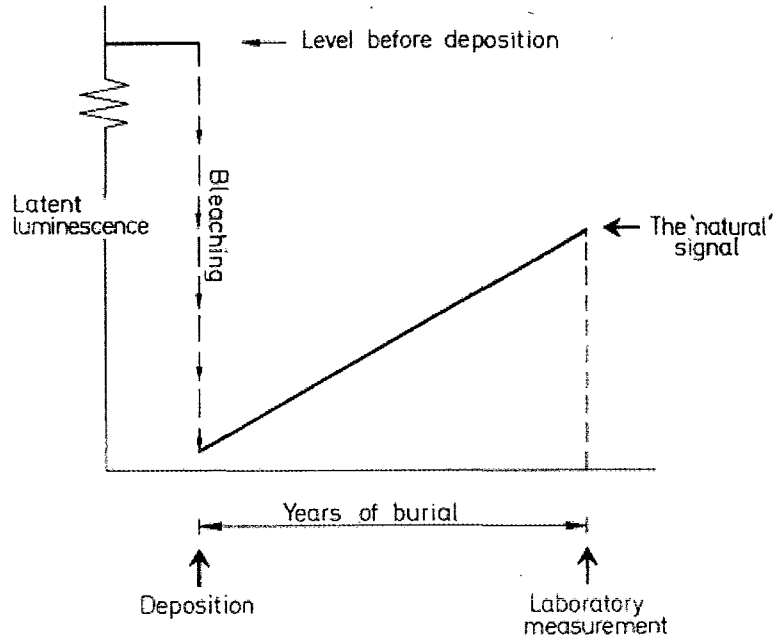

Figure 1. The OSL signal from most recent bleaching event to laboratory measurement (Aitken, 1998).

neutrons. The OSL signal from a sample is proportional to the total energy absorbed during burial unless saturation is reached, meaning that all available trapping states are occupied.

Within a volume with dimensions greater than the range of the relevant radiation, the overall rate of energy absorption is equal to the rate of emission. Using this relationship, the dose rate can be calculated from the concentration of radioelements in the sample. These concentrations can be determined using analytical techniques such as neutron activation analysis (NAA), atomic absorption, x-ray fluorescence, inductively-coupled plasma mass spectrometry (ICPMS), and flame photometry (applicable only to potassium measurements). In the concentration approach to dose rate determination, the potassium, thorium, rubidium, and uranium contents of the sample are measured, and dose rates are determined from standard conversion tables. The dose rates determined in this manner can be inaccurate if the thorium and uranium decay chains are not in equilibrium, so this should be verified using a high-resolution gamma spectrometer or an alpha spectrometer. While quartz, feldspar, and clay minerals all have similar mass absorption

coefficients, water has a higher mass absorption coefficient, so accurate dose rate determinations also depend on knowledge of the moisture content of samples.

Samples are collected and analyzed for a number of purposes, including the estimation of paleodose, dose-rate, and moisture content. Care must be taken to ensure that any samples intended for paleodose estimation are not exposed to daylight. Sample processing must also be done in semi-darkness, using red, orange-yellow, or yellow-green light. Although shorter wavelength light, such as the latter, tends to bleach the sample, it can be used at lower intensity than red light since the eye is more sensitive in that range.

For samples with grain sizes of 0.01 mm or less, the age of the sample is calculated from the paleodose measured in the laboratory and the calculated alpha, beta, gamma, and cosmic ray dose rates ($\dot{D}_\alpha, \dot{D}_\beta, \dot{D}_\gamma$, and $\dot{D}_c$) as

$$Age = \frac{Paleodose}{k\dot{D}_\alpha + \dot{D}_\beta + \dot{D}_\gamma + \dot{D}_c} \quad (1)$$

where $k\dot{D}_\alpha$ is the effective alpha contribution. The constant k is introduced to compensate for the fact that the induced luminescence per unit radiation dose is lower for alpha particles than for beta particles and gamma rays (Aitken, 1985). In coarse-grain dating, the 'rind' of the grain is etched with hydrofluoric acid, rendering the external alpha contribution negligible. Equation 1 then becomes

$$Age = \frac{Paleodose}{0.90\dot{D}_\beta + \dot{D}_\gamma + \dot{D}_c} \quad (2)$$

The $0.90\dot{D}_\beta$ 0.90 term reflects the attenuation of the beta contribution in the rind of the grain, which is removed during etching (Aitken, 1998).

The dose rates used in the laboratory exceed natural environmental dose rates by a factor of more than 10^8. A gamma-ray source with high enough activity to provide a dose rate sufficient for dating would require heavy shielding; since beta radiation has the same efficiency for inducing luminescence as gamma rays, beta sources are typically used (Aitken, 1985). The beta source will often be calibrated to a known gamma-ray source, and gamma-ray sources are also commonly used for the bulk irradiation of samples. In quartz, variations in dose response due to dose-rate effects may be significant for dose rates as low as 10 Gy/min, so rates less than or equal to 1 Gy/min are typically used for dating. This effect most likely arises from competition between the dosimetric OSL traps and shallow traps, since the occupancy of the shallow traps depends on the balance between the rate of filling and the rate of loss as the sample regains thermal equilibrium (Aitken, 1985). At high dose rates, more of the shallow traps are occupied during irradiation, resulting in more rapid filling of the OSL traps than would occur in nature. If irradiation is carried out at a slightly elevated temperature, the electron-retention lifetime of the shallow traps is reduced. This has the effect of keeping the concentration of electrons in the shallow traps low, more in keeping with that expected during low dose-rate irradiations. An additional complication, discussed in Section 2.4.4, arises from the fact that paleodose determined by laboratory irradiation of the sample will be an underestimate of the actual dose if the lifetime of the trapped electrons is not significantly greater than the age of the sample (Aitken, 1998).

Heavy liquid separation is used to isolate the quartz and feldspar fractions before analysis. Samples weighing a few mg are deposited in a monolayer on aluminum or steel discs 10 mm in diameter and 0.5 mm thick. All samples are normally heated before measurement, and some procedures insert a delay of a day or more between irradiation and preheating, or between

preheating and measurement, in order to allow the crystal lattice to relax. The appropriate preheat procedure for a sample can be determined by looking at its TL glow curve, or through a preheat plateau test, which consists of a series of paleodose measurements made using preheats of increasing temperature. The optimal preheat temperature is the lowest temperature at which a consistent paleodose estimate is achieved; in other words, the "plateau" of the paleodose versus preheat temperature graph (Aitken, 1998). The use of a preheat is important to eliminate thermally unstable portions of the laboratory-induced signal (as would happen over time with storage at room temperature), and will cause a certain amount of erosion of the natural signal as well, which is acceptable so long as the signal is not seriously depleted (Bøtter-Jensen *et al.*, 2003b, Aitken, 1998).

2.2.2 Accident dose estimation

Many of the principles behind geological and archaeological dating apply equally to retrospective accident dosimetry. In general, fired ceramics are most suitable for retrospective dosimetry, including common building materials such as bricks, floor tiles, and roof tiles, and household objects and fixtures like porcelain toilets and bathtubs, pots and dishes, lamp holders, and power line insulators (Bøtter-Jensen *et al.*, 2003b). The OSL signal of these materials is reset by firing during the manufacturing process, and the 'paleodose' absorbed from natural radioelements since manufacture must be estimated and subtracted (Aitken, 1998). TL analysis of porcelain for accident dose reconstruction was first performed using samples from fallout regions surrounding Hiroshima (Stoneham, 1984). Because brick has been found to absorb radionuclides from rainwater in high fallout areas, porcelain is often preferred for dose evaluation (Adamiec *et al.*, 1997). Sampling of materials from a variety of locations and at a variety of depths in materials such as brick can provide additional information on the nature of

the radiation field and the amount of shielding provided by the structure (Bøtter-Jensen *et al.*, 2003b).

Bricks generally contain large amounts of quartz and some quantity of feldspar; for accurate dose estimation, particularly when the variation of dose with depth in brick is being studied, a homogeneous distribution of quartz grains within the brick is crucial (Bøtter-Jensen *et al.*, 2003b). In more modern buildings, quartz grains in bricks are not in the appropriate size range for analysis; in some cases, infrared stimulated luminescence (IRSL) of feldspar from such bricks has been successfully used for dose reconstruction (Niedermayer *et al.*, 2000). As with geological dating, care must be taken to avoid exposing the sample to light prior to measurement. Surface material that may have been exposed to light must be removed, but may be retained for particle size analysis and internal dose rate determination. In preparation for OSL analysis, samples are sliced into sections and crushed before sand-sized (90-180 μm) grains are extracted through sieving. Heavy-liquid separation is used to concentrate the quartz grains, following which any remaining feldspar contamination is eliminated through etching in 40% HF (Bøtter-Jensen *et al.*, 2003b).

Mineral grains within bricks will accumulate an absorbed dose of up to 5 mGy a^{-1} due to the presence of naturally-occurring radionuclides; in older buildings, this may amount to a large proportion of the total accrued dose. The task, then, is to accurately estimate this background dose in order to determine the additional dose accrued due to accidental (or intentional) exposure (Bøtter-Jensen *et al.*, 2003b). To accomplish this, the natural dose rate must be measured and the age of the building (or more specifically, the age of the bricks) estimated. The dose rate from radioactive impurities within individual quartz grains is generally negligible (Aitken, 1985), so the main contribution is from ^{40}K, ^{232}Th, and ^{238}U (and progeny) present in the surrounding

material (Bøtter-Jensen *et al.*, 2003b). The dose rate can thus be measured using the same techniques as in geological dating, as described in section 2.2.1. Short-term measurements of the background dose rate can also be made using Al_2O_3:C dosimeters and compared with the results obtained from the measured concentrations of naturally-occurring radionuclides (Bøtter-Jensen *et al.*, 1999).

The total absorbed equivalent dose includes contributions from accidental and background exposure, and is expressed as follows:

$$D_e = D_a + t(\dot{D}_\alpha + \dot{D}_\beta + \dot{D}_\gamma + \dot{D}_c)_D \qquad (3)$$

that is, the total absorbed dose is the sum of the accident dose, D_a, and the background dose, given by the product of the total annual background dose from alpha ($\dot{D}_\alpha D$), beta ($\dot{D}_\beta D$), gamma ($\dot{D}_\gamma D$), and cosmic ray ($\dot{D}_c D$) radiation and the time t since manufacture (in years) (Bøtter-Jensen *et al.*, 2003b). Through computational modelling, conversion factors can be calculated to relate the estimated accident dose in the quartz grains to a dose in air at a selected location (Bailiff and Stepanenko, 1996).

Additional information about the type and energy of the incident radiation can be obtained through the measurement of dose-depth profiles in brick; in fact, an instrument has been developed to allow continuous scanning of core samples for this type of analysis (Bøtter-Jensen *et al.*, 1995). Using measurements from bricks irradiated in the laboratory using calibrated gamma sources as well as Monte Carlo simulation techniques (Bøtter-Jensen *et al.*, 1999, Bailiff and Stepanenko, 1996), dose-depth profiles can be used to validate the conversion of dose in brick to dose in air (or tissue) at a reference location (Bøtter-Jensen *et al.*, 2003b).

2.3 Luminescence theory

Optically stimulated luminescence belongs to a category of phenomena known as stimulated relaxation phenomena (SRP); those phenomena that result in the emission of light are known as stimulated luminescence phenomena (Bøtter-Jensen *et al.*, 2003b). By definition, luminescence is light emitted following the absorption of some form of external energy, and includes all processes that convert non-thermal energy into light (Bøtter-Jensen, 2000). If the delay between the absorption of energy and the emission of the luminescence (the characteristic lifetime, τ) is less than 10^{-8} s, the process is termed fluorescence, while light emission following delays on the order of a few seconds or more is termed phosphorescence. For values of τ where the distinction is not clear, the temperature dependence of the process can be used as a guide: phosphorescence is a temperature-dependant process, while fluorescence is not (McKeever, 1985).

It should be noted that the terms "thermoluminescence" and "optically stimulated luminescence" are somewhat misleading, since they refer to the type of energy used to liberate charge from the metastable state and not the energy responsible for the excitation (Chen and McKeever, 1997). The excitation energy is provided by ionizing radiation in the case of TL and OSL, although it is certainly possible that, for example, a (mechanically-induced) triboluminescence signal could be observed during thermal or optical stimulation. Photoluminescence (PL) is related to OSL in the sense that materials that produce OSL will also produce PL, but as a rule the intensity of the photoluminescence will not be affected by irradiation of the sample (Bøtter-Jensen *et al.*, 2003b). In PL, electrons in crystal defects are excited via the absorption of visible or UV light, with the light emitted during relaxation at a longer wavelength than that of the stimulating light, according to Stokes' law (McKeever, 1985). The intensity of the emission is dependent upon

the concentration of excited defects; in the case where these defects are created through irradiation, the PL signal will vary with absorbed dose, and is referred to as radiophotoluminescence (Bøtter-Jensen *et al.*, 2003b).

2.3.1 Mechanism and models

During irradiation, energy absorbed by an insulator or semiconductor results in the excitation of free electrons and free holes (Bøtter-Jensen *et al.*, 2003b). These electronic species may then be trapped at defects within the material, with defects typically caused by the dislocation of negative ions, resulting in negative ion vacancies that act as electron traps (Bøtter-Jensen, 2000, Bøtter-Jensen *et al.*, 2003b). The excitation of charge occurs mainly through the Compton effect or the photoelectric effect, depending on the type and energy of the incident radiation, and the system is left in a metastable state. During stimulation, the trapped charge absorbs external energy, resulting in the relaxation of the system and return to equilibrium. Trapped electrons and holes are released and recombine, and in some cases the recombination may be radiative, causing the emission of luminescence (Bøtter-Jensen *et al.*, 2003b).

There are thus three stages that must occur in order for OSL to be observed:

1. Excitation, in which ionizing radiation excites electrons from the valence band to the conduction band, where they are trapped in metastable localized states at defects in the material;
2. Storage, during which electronic species remain localized, with mean lifetimes in these metastable states dependent upon the energy depth of the trap; and,
3. Stimulation, in which light ionizes the defects and electronic species recombine, resulting in the emission of luminescence.

The excitation and stimulation stages of the process are illustrated in Figure 2. During excitation (a), ionizing radiation results in the excitation of electrons to the conduction band. Some of these may be trapped in 'shallow traps' (1); these may be de-trapped through thermal vibrations of the lattice and return to the conduction band. Others will be localized in dosimetric traps (2) or deep traps (3). While charge is readily liberated from dosimetric traps upon stimulation, the energy provided by the stimulation light may be insufficient to free electrons from deep traps. Some may recombine with trapped holes (4), resulting in the emission of light during irradiation (radioluminescence). During stimulation (b), light ejects electrons from the dosimetric traps (2), after which they may undergo radiative recombination (4) or be re-trapped in shallow (1) or deep (3) traps (Bøtter-Jensen *et al.*, 2003b).

The intensity of the luminescence emitted in OSL depends on the system's rate of return to equilibrium, which in turn depends on the trapped charge concentration. In OSL measurements, the intensity of emitted luminescence is measured as a function of stimulation time, resulting in a curve whose integral is proportional to the absorbed radiation dose (Bøtter-Jensen *et al.*, 2003b).

(a) Excitation (irradiation)

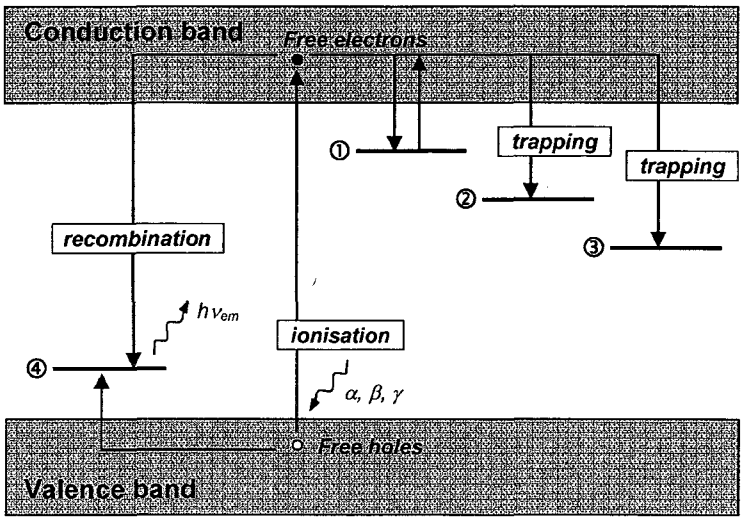

(b) Stimulation

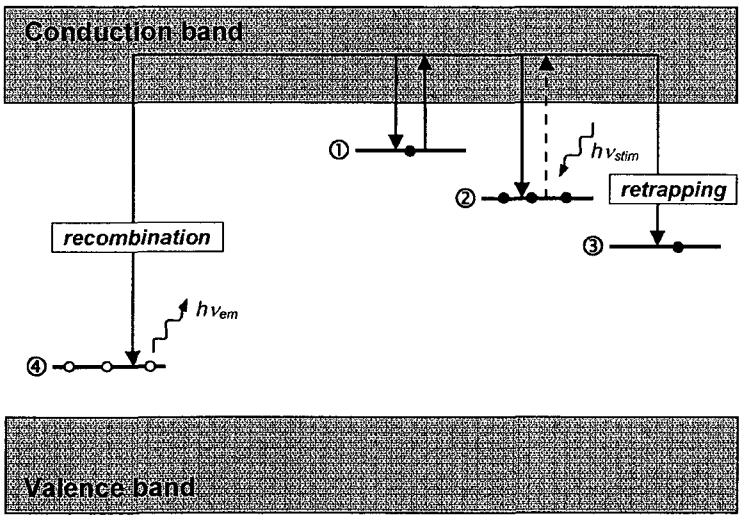

Figure 2. Flat-band diagram of transitions during (a) irradiation and (b) stimulation of crystals.

When the stimulation is thermal, p represents the probability at fixed temperature of return to equilibrium through thermal ionisation of the metastable state, and the function has the form

$$p(E,s,T) = s\exp\left\{-\frac{E}{kT}\right\} \tag{4}$$

where k is the Boltzmann constant, E is the "trap depth" and s (with dimensions of inverse time) is alternately known as the pre-exponential factor or the "attempt-to-escape frequency" (Aitken, 1998). The parameters characterising the metastable states are thus E and s. In TL measurements, T varies with time according to $T(t) = T_0 + \beta t$ (where β is the heating rate), producing a characteristic "glow curve".

In the case of optical stimulation, p depends on the photoionisation cross-section, discussed further in Section 2.3.2, so

$$p(h\nu) = \Phi\sigma(E_0) \tag{5}$$

where Φ is the intensity of the stimulating light, and $\sigma(E_0)$ is the photoionisation cross-section for a defect of ionisation threshold energy E_0. The relevant state parameter is, therefore, E_0 (Bøtter-Jensen *et al.*, 2003b).

2.3.2 The photoionisation cross-section and rate equations

The photoionisation cross-section determines the likelihood of charge escaping a trap during optical stimulation, and as such is the single most important parameter governing OSL transitions (Bøtter-Jensen *et al.*, 2003b). For a defect-band optical transition, the absorption coefficient, $\alpha(h\nu)$, can be written as the product of the concentration of defects, $n(E_0)$, and the photoionisation cross-section for photons of energy $h\nu$, $\sigma(h\nu, E_0)$:

$$\alpha(h\nu, E_0) = n(E_0)\sigma(h\nu, E_0) \tag{6}$$

A number of expressions for $\sigma(h\nu, E_0)$ have been proposed, each based on different assumptions regarding the potential surrounding the defect (Bøtter-Jensen *et al.*, 2003b). For the case of a shallow trap, a potential based on that for an electron in a hydrogen-like atom is assumed, so for a free electron in a plane wave state, the photoionisation cross-section can be written

$$\sigma(h\nu, E_0) \propto \frac{(h\nu - E_0)^{3/2}}{(h\nu)^5} \tag{7}$$

A delta-function potential is more appropriate for deep traps, where the potential barrier preventing electrons from escaping from the trap is much greater, so the expression becomes

$$\sigma(h\nu, E_0) \propto \left[\frac{4(h\nu - E_0)E_0}{(h\nu)^2}\right]^{3/2} \tag{8}$$

When optical stimulation is at constant wavelength and intensity, p does not vary with time, and the resulting luminescence is known as continuous wave OSL (CW-OSL). If the intensity is varied with time according to the equation

$$\Phi(t) = \Phi_0 + \beta_\Phi t \tag{9}$$

where $\beta_\Phi = d\Phi / dt$ is constant, the recorded luminescence is termed linear modulation OSL (LM-OSL). Stimulation light may also be "pulsed" by starting and stopping stimulation at regular intervals; this is known as pulsed OSL (POSL). One advantage of POSL is that luminescence may be detected between pulses, eliminating the need to use filters to prevent stimulation light from entering the detection system, and increasing detection efficiency by allowing emitted luminescence to be detected over a wider range of wavelengths.

The many energy-level transitions occurring during irradiation and stimulation, as illustrated in Figure 2, result in a complicated series of coupled non-linear rate equations. For simplicity, the basic model considers a system with only one electron trap and one hole trap, with recombination occurring at the hole trap, as depicted in Figure 3 (a) (Bøtter-Jensen *et al.*, 2003b). Figure 3 illustrates some additional complexities that can be introduced into the model: a competing deep trap (b), a competing shallow trap (c), and an additional, non-radiative, recombination centre (d) (Chen and McKeever, 1997).

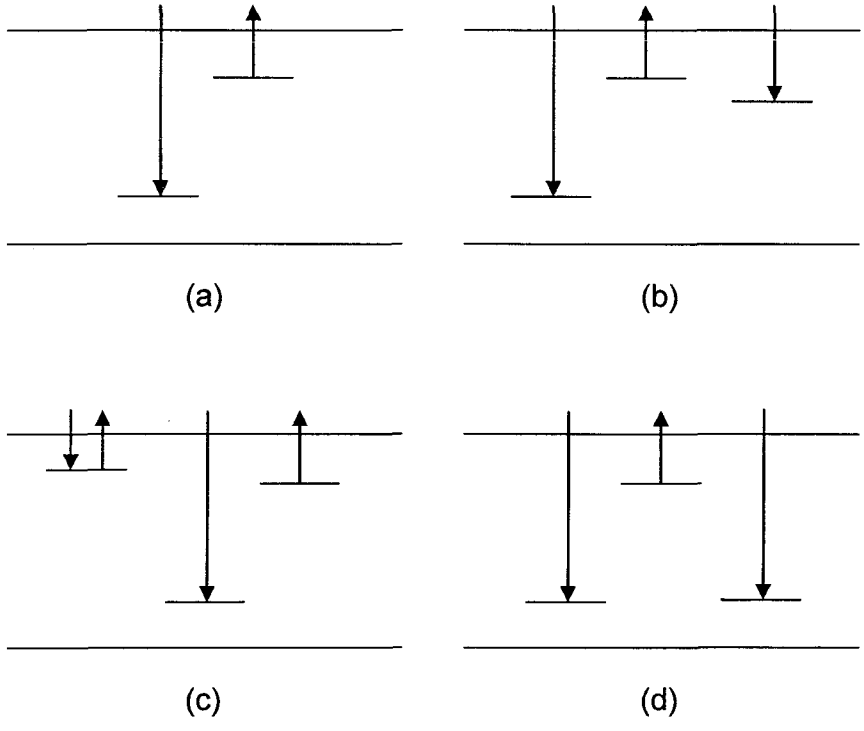

Figure 3. OSL models: (a) One-trap/one-centre model, (b) Model with additional deep trap, (c) Model with competing shallow trap, (d) Model with non-radiative recombination centre (after Chen and McKeever, 1997).

Detailed derivations of rate equations for various models and stimulation modes are found in Bøtter-Jensen *et al.* (2003b). For the one-trap/one-centre model, charge neutrality requires that $n_c + n = m_v + m$, where n_c and n are the concentrations of electrons in the conduction band and

the traps, and m_v and m are the concentrations of holes in the valence band and recombination centres. Assuming that $n_c = m_v = 0$ immediately following irradiation when the system is in thermal equilibrium, we have $n_0 = m_0$ at the start of optical stimulation. When electrons are stimulated from the traps (before recombination), $n_c + n = m$, so the rate of change of these concentrations is

$$\frac{dn_c}{dt} = -\frac{dn}{dt} + \frac{dm}{dt} \tag{10}$$

The rate of change of the concentration of electrons in the traps can be expressed as the rate of stimulation of electrons from the traps minus the rate of re-trapping of electrons, and the rate of change of the concentration of holes is simply the recombination rate. Using the "quasi-equilibrium" assumption that the population of free electrons in the conduction band is relatively constant, $dn_c/dt << dn/dt$, dm/dt and $n_c << n$, m, *so* we have

$$\frac{dn}{dt} = \frac{dm}{dt} \tag{11}$$

It is assumed that the rate of re-trapping is slow compared to the rate of stimulation from the traps and the rate of recombination. The rate of stimulation from the traps is thus equal to the recombination rate, which in turn is equal to the intensity of the OSL emission, I_{OSL}, so

$$I_{OSL} = -\frac{dm}{dt} = -\frac{dn}{dt} = np \tag{12}$$

where p is the rate of stimulation of electrons from the trap (Bøtter-Jensen *et al.*, 2003b). The solution to this first-order model is a simple exponential decay with initial OSL intensity I_0 and OSL decay constant τ_d:

$$I_{OSL} = n_0 p e^{-tp} = I_0 e^{-\frac{t}{\tau_d}} \quad I_{OSL} = n_0 p \exp\{-tp\} = I_0 \exp\{-t/\tau_d\} \tag{13}$$

In practice, this simple model is insufficient to explain the OSL behaviour of most materials, and serves only as an illustration of a simple one-trap/one-centre model. CW-OSL curves do not generally show simple exponential decay behaviour, but rather exhibit a variety of shapes – all monotonically decreasing as stimulation depletes the trapped charge. Some of these variations can be explained even with the simple one-trap/one-centre model if re-trapping is no longer neglected (Bøtter-Jensen *et al.*, 2003b). The resulting equations are explored in detail by Chen and Leung (2003), who demonstrate that the resulting OSL curve is best represented by a "stretched exponential" of the form

$$I_{OSL} = I_0 \exp\left\{-(t/\tau_d)^{\beta}\right\}, \; 0 < \beta < 1 \tag{14}$$

The validity of this representation is illustrated by a fit to an actual OSL decay curve in Section 4.1 A description of a more generalized model, considering all of the processes shown separately in Figure 3, can be found in McKeever *et al.* (1997a).

2.4 Dose estimation

2.4.1 Signal resetting

The OSL signal in a material can be zeroed by heating or by exposure to light. In geological dating, the age determined through analysis represents the time elapsed since the signal in the sediment was last zeroed by exposure to light; in other words, the burial time. Depending on the way in which the sediment was deposited, the degree of zeroing will vary; Aeolian sediments are generally much more well-bleached than are fluvian deposits. In accident dose estimation, the zeroing event will normally be the firing of a building material (such as a brick) or a porcelain

fixture during manufacture. An advantage of using recently-manufactured items, such as cellular phone components, for retrospective dosimetry is that the initial accumulated dose is likely to be negligible relative to biologically significant doses.

2.4.2 The regenerative approach

All OSL measurement protocols are concerned with estimating the equivalent dose (D_e) of a sample, defined here as the laboratory beta dose required to produce an OSL signal equivalent to the accident dose or natural environmental dose. The measurement protocols used can be divided into broad categories according to the number of samples required to arrive at an estimate of the natural dose, e.g., multiple aliquot protocols and single aliquot protocols. The first term refers to methods requiring the analysis of a number of aliquots, or notionally identical sub-samples of a larger sample, while the second covers methods allowing dose estimates through analysis of a single aliquot. These procedures may be further qualified as additive-dose methods, where the samples are exposed to an additional known dose prior to measurement, or regenerative-dose methods, where the natural signal of the sample is measured before at least one regeneration dose (roughly equal to the natural dose) is administered and the signal measured again (Bøtter-Jensen *et al.*, 2003b).

The experiments in this work use only single aliquot protocols, where repeated measurements are performed on each aliquot, thus requiring smaller samples than multiple-aliquot methods. There are several advantages to this type of method, including increased precision and elimination of the need for normalization between samples. The improvement in precision is gained because the dose estimate is based on a number of measurements of a single aliquot, eliminating the uncertainty introduced by the actual differences in sensitivity and dose response between "notionally" identical aliquots taken from a sample. Initially, single-aliquot protocols were not

widely used due to changes in the luminescence response of materials over cycles of irradiation and read-out (Bøtter-Jensen *et al.*, 2003b). Further study of these sensitivity changes revealed that they are caused by the transfer of charge between competing traps and recombination centres (Jungner and Bøtter-Jensen, 1994, McKeever *et al.*, 1996b, McKeever *et al.*, 1997b).

The single-aliquot additive-dose (SAAD) protocol was proposed by Murray *et al.* (1997). This procedure involves repeated cycles of preheating, measurement, and irradiation, where the OSL signal is only partially depleted by a brief (0.1-0.2 s) measurement and an additive dose is given between measurements (Murray *et al.*, 1997). While SAAD and other additive-dose procedures were developed early on (Duller, 1991, Galloway, 1996), the single-aliquot regenerative-dose (SAR) protocol has recently gained more widespread use, and is used exclusively in the work reported here (Murray and Roberts, 1998, Murray and Wintle, 2000).

In principle, regenerative methods are straightforward. The OSL signal from the sample is measured (L_n), depleting the charge in the light-sensitive traps. Following the initial measurement, a calibration dose (commonly referred to as a regeneration dose, D_r, roughly equal to the natural dose) is given, and the signal measured once more (L_r). If there is no change in sensitivity between measurements, the natural dose is simply given by $D_e = \frac{L_n}{L_r} D_r$. In practice, sample treatment such as pre-heating to remove thermally unstable OSL signals does result in a significant change in sensitivity. A correction can be made by normalising the OSL signal to the signal from a small test dose administered following each measurement. Each test dose signal has been demonstrated to be proportional to the sensitivity applicable to the preceding OSL measurement, so the ratio between the latter and the OSL from the test dose yields a result independent of sensitivity change (Murray and Mejdahl, 1999).

The SAR protocol is capable of producing an estimate of absorbed dose from as few as four OSL measurements on a single sample. After preheating to a fixed temperature (usually in the range of 180-280°C for quartz), the initial OSL signal (natural + accident dose) is measured, with L_0 representing the integrated counts over the first few seconds of illumination. Following this measurement, the sample is cooled and given a test dose, selected as approximately 10-20% of the natural dose, with the same test dose being used in all subsequent measurements. The sample is then heated to remove thermally-unstable luminescence (in quartz, arising from the 110°C TL trap), and the OSL response to the test dose is measured (T_0). This sequence is repeated for at least one regeneration dose and subsequent test dose (giving L_r and T_r). If the dose response curve is linear over the relevant range, the natural dose can be calculated from these four measurements as

$$D_e = \left(\frac{L_0}{L_r}\right)\left(\frac{T_r}{T_0}\right)D_r \tag{15}$$

A typical analysis sequence for a quartz sample is outlined in Table 1. With the appropriate choice of at least three regeneration doses, D_e can be determined by interpolation, eliminating the requirement for linearity of dose response.

Table 1. A typical SAR sequence for a quartz sample (Bøtter-Jensen *et al.*, 2003b, Murray and Wintle, 2000)

Step	Dose measured	Treatment	Observed
1	Natural + accident dose (D_e)	Preheat (180-280°C for 10 s)	
		OSL at 125°C	L_0
		Test dose, Preheat (160°C)	
		OSL at 125°C	T_0
2	Regeneration dose 1 ($D_1 < D_e$)	As in step 1	L_1, T_1
3	Regeneration dose 2 ($D_2 \cong D_e$)	As in step 1	L_2, T_2
4	Regeneration dose 3 ($D_3 > D_e$)	As in step 1	L_3, T_3
5	Regeneration dose 4 ($D_4 = D_1$)	As in step 1	L_4, T_4
6	Regeneration dose 5 ($D_5 = 0$ Gy)	As in step 1	L_5, T_5

Typically, the first regeneration dose is repeated as a check for the accuracy of the sensitivity correction. In addition, a "zero-dose" signal is measured, which can also serve to indicate the degree to with charge may be transferred from optically insensitive traps to OSL traps through thermal assistance (Bøtter-Jensen *et al.*, 2003b). A growth curve resulting from the SAR procedure described in Table 1 is illustrated in Figure 4. The sensitivity-corrected signal, S_i, is given by the ratio of the OSL responses to the regeneration (or natural) dose and the following test dose, so $S_i = L_i/T_i$.

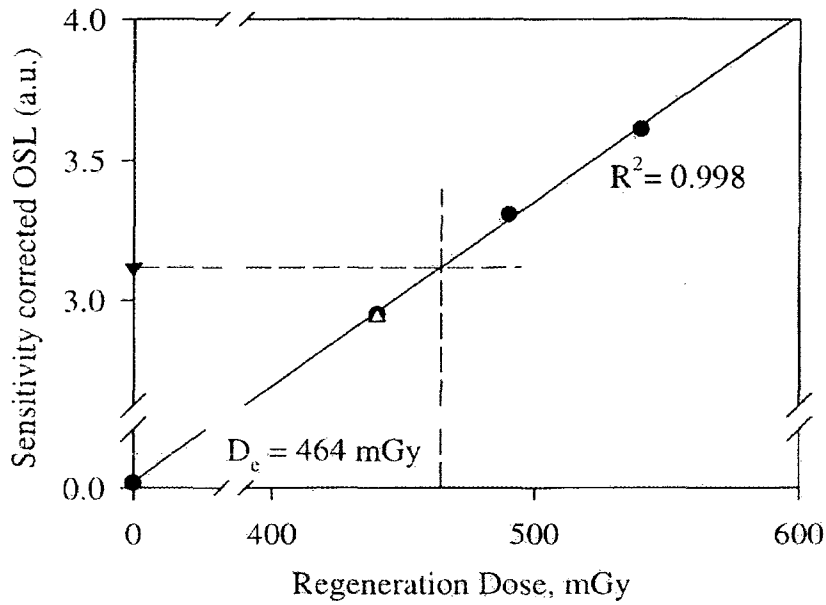

Figure 4. SAR OSL growth curve for a quartz sample from Chernobyl. ▼ - natural OSL, ● - regenerated OSL, △ - repeated regeneration dose. (Bøtter-Jensen *et al.*, 2003b)

2.4.3 Choice of OSL signal

As a rule, for a constant signal, the counts observed over equal periods will vary such that if the true average number of counts is N, 68% of the observations will fall in the range of $N \pm \sigma$, where $\sigma = \sqrt{N}$. Alternatively, if N is the actual number of counts, there is a 68% likelihood that the true mean lies within $\sqrt{N}$ of this value. This is a good approximation when N is large (> 20), as is invariably the case for OSL signals used in dosimetry (which should ideally have > 1000 integrated counts). A consequence of this approximation is that short shines with low total counts produce measurements with relatively large uncertainties (Aitken, 1998). The effect of statistics on the choice of OSL signal for analysis is discussed further in Section 3.3.1.

A photomultiplier tube with a bi-alkali photocathode typically has a dark current of 20-50 counts per second (cps), so this generally represents the single largest contribution to the background signal; however, this effect is highly dependent on the ambient temperature, and for an increase

in temperature from 20°C to 30°C, the dark current may nearly double. Another source of background noise is filter breakthrough, which may contribute 2-20 cps. This is observed when the tail of the stimulation light's transmission filter overlaps with the acceptance window of the filter between the sample and photomultiplier tube. Late-light subtraction is often used to correct for these effects; that is, subtraction of the light emitted at the end of illumination from the total luminescence signal, which includes subtraction of the filter breakthrough and dark current components as well as any time-independent phosphorescence and hard-to-bleach components of the signal (Aitken, 1998).

There is some question of which part of the OSL decay curve should be used for the evaluation of D_e. The first few seconds (or fractions of seconds) of the OSL curve correspond to the emptying of the most optically-sensitive traps, and provide a better signal-to-noise ratio than the integrated luminescence over the duration of the measurement (Bøtter-Jensen *et al.*, 2003b). Banerjee *et al.* (2000) proposed an analysis method based on the subtraction of a background calculated from the signal observed at the end of stimulation. They proposed an estimate of the random uncertainty given by

$$\sigma = \frac{\sqrt{\sum_i S_i + 2\overline{B}n}}{\sum_i S_i - \overline{B}n} \tag{16}$$

where S_i is the signal from the ith channel (of channels 1 through n) and $\overline{B}$ is the average background. Under this definition, the uncertainty in the background-corrected signal for a "dim" quartz sample (50 or fewer counts in the first 0.24 s from a dose of 50 mGy) is minimized by using approximately the first 7 s of the signal, while this uncertainty is relatively constant

with integration time for a "bright" sample (~4000 counts in the first 0.24 s) (Banerjee *et al.*, 2000).

2.4.4 Signal stability

Luminescence techniques, especially as applied to dating, are fundamentally limited by the rate of thermal eviction of electrons from traps. The concentration of trapped electrons remaining at time t, assuming an initial concentration N_0, is given by

$$N = N_0 \exp\left(-\frac{t}{\tau}\right) \tag{17}$$

where τ is the characteristic lifetime of the electron in the trap. Keeping in mind that a sample is continuously irradiated during burial, τ must be at least 10 times the age of the sample to avoid an underestimation of the sample's age by more than 5% (or 20 times for a 2% age shortfall) (Aitken, 1998).

In TL dating, the plateau test is used to ensure that the traps are adequately stable – if traps (or TL peaks) with different lifetimes result in the same value for the paleodose, they are assumed to be sufficiently long-lived. A similar plateau test can be used in OSL measurements to select a preheat temperature resulting in a stable estimate of D_e. Smith *et al.* (1990) calculated the lifetime of the quartz OSL signal as falling in the range of 200-1800 Ma at 20°C. A more detailed study by Huntley *et al.* (1996) determined that four different traps contributed to the OSL signal, with lifetimes of 14 ka, 2 Ma, 28 Ma, 4700 Ma respectively; they used an analysis procedure incorporating a preheat to 160°C for 48 h to eliminate any contribution from the 14 ka traps.

In certain materials, most notably K-feldspars, the luminescence signal is known to decrease as time elapses following irradiation. The rate of decrease is much greater than that predicted by the mean lifetimes of electrons in the relevant defects as calculated from the physical model (Huntley and Lamothe, 2001). In other words, the fading is far in excess of the expected thermal fading described above; for this reason, the phenomenon is termed 'anomalous fading'(Aitken, 1998). It was first observed in the TL dating of feldspars and polymineral fine grains extracted from lava flows (Wintle, 1973). Since luminescence induced by laboratory irradiation does not exhibit fading to the same extent as the natural luminescence signal, failure to account for the effects of fading results in an underestimate of D_e. The degree of underestimation is sample-dependent, and varies significantly (Aitken, 1998).

Detailed treatments of anomalous fading are found in Aitken's books on TL dating and optical dating (1985, 1998). The most widely accepted mechanism for this phenomenon is quantum-mechanical tunnelling. This means that electrons have some small probability of escape other than via the conduction bands, and that this probability does not increase with temperature (Aitken, 1998). The tunnelling model predicts that the rate of recombination through this mechanism is inversely proportional to the time since irradiation (Huntley and Lamothe, 2001); integration shows that the remaining population of trapped electrons decreases logarithmically with time, as observed by Visocekas (1985). Anomalous fading data for a number of K-feldspar samples is presented in Figure 5.

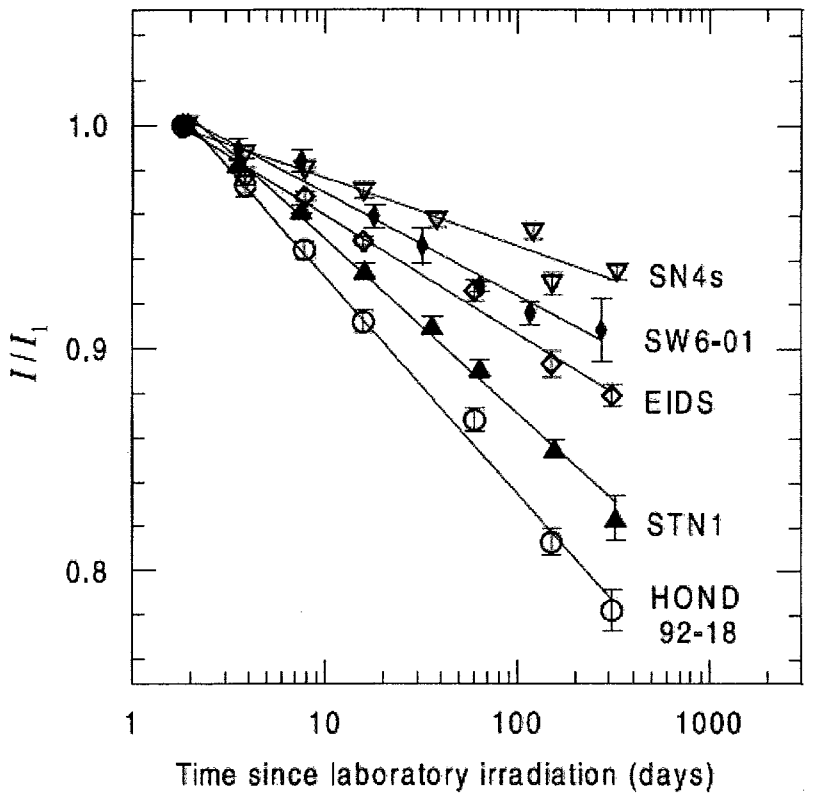

Figure 5. Anomalous fading data for K-feldspar samples. I_1 is the luminescence intensity of the first measurement, taken 1.8 days following irradiation. From Huntley and Lamothe (2001).

Huntley and Lamothe (2001) have studied fading in K-feldspars in detail, measuring fading rates of 2% to 10% per decade, meaning a factor of ten increase in the time since irradiation. The intensity at time t is then given relative to the intensity at an arbitrary time t_c as

$$I(t) = I_c\left[1 - \frac{g}{100}\log_{10}\left(\frac{t}{t_c}\right)\right] \tag{18}$$

where g is the fading rate in %/decade. Huntley and Lamothe (2001) use this model to correct optical ages for fading through laboratory measurement of the g factor, with results in good agreement with independent age determinations. Another method successfully used for fading correction, known as the *fadia* method, involves measuring the variation in fading rates among single grains in order to extrapolate to zero fading (Lamothe and Auclair, 1999, Lamothe and Auclair, 2000).

2.5 Material characteristics

2.5.1 Natural materials

Quartz

Quartz, the most common mineral in the Earth's crust, is found in granite, volcanic rocks, and sedimentary deposits. Sediments containing quartz are commonly incorporated into bricks and pottery, meaning that the OSL properties of quartz can be exploited for applications ranging from quaternary geological dating and archaeological dating to accident dose reconstruction (Bøtter-Jensen *et al.*, 2003b). Within the last decade, the SAR procedure has had an enormous impact on the approach to dating and retrospective dosimetry using quartz; the advantages of this procedure are discussed in Section 2.4.2. Quartz can absorb doses on the order of 100 Gy before saturation is reached, making it useful for dating sediments up to several hundred thousand years old; it is also sensitive enough to be used to measure doses as low as 10 mGy in fired materials (Bøtter-Jensen *et al.*, 2003b). For these reasons, it is the most widely studied natural material, and the most widely used for geological and archaeological dating, as well as retrospective dosimetry.

Feldspar and other natural materials

Feldspars are composed of tetrahedral units of AlO_4 and SiO_4, with the sharing of oxygen molecules between adjacent tetrahedrals in the lattice. Cations, such as K^+, Na^+, and Ca^{2+}, are incorporated in the crystal structure; these, and a variety of other substitutional impurities, contribute to the luminescence properties of the material. Depending on their composition, feldspars are classified as plagioclase or alkali, with the later being potassium-rich and lighter than plagioclase feldspars (Bøtter-Jensen *et al.*, 2003b). While quartz OSL is generally

measured using visible light (often blue-green), infrared light is most often used as the stimulation source for feldspars, with the resulting emission referred to as infra-red stimulated luminescence (IRSL). Feldspar also produces OSL under visible light stimulation, although it is likely that the OSL and IRSL signals arise from different (but overlapping) sets of traps (Duller and Bøtter-Jensen, 1993). As with quartz, continuous wave IRSL decay curves from feldspar are non-exponential; they exhibit a slower decay than OSL from quartz, and have been approximated by power functions of the form $(1 + Bt)^{-P}$, where $1 < P < 2$ (Bailiff and Poolton, 1991). Nearly all feldspars have been shown to exhibit anomalous fading (Huntley and Lamothe, 2001), as described in Section 2.4.4.

Although quartz and feldspar are the dominant materials in retrospective dosimetry, other natural materials have been examined, including calcium fluoride (Chougaonkar and Bhatt, 2004) and biotite, a type of mica (Li and Yin, 2006). Bailey *et al.* (2000) have reported on the use of the UV emission of NaCl in dating and retrospective dosimetry. The dose response was demonstrated to be well-represented as a sum of two exponentials approaching saturation above 60 Gy, and the thermal stability of the OSL signal was estimated to permit dating to at least 10 ka. The extreme solubility of NaCl means that the resetting event may be dissolution, with the date obtained through analysis representing the date of desiccation.

2.5.2 Synthetic materials

Al_2O_3:C

Anion-defective α-Al_2O_3:C crystals were first developed in Russia at the Urals Polytechnical Institute by Akselrod *et al.* (1990) for TL dosimetry. The intention was to improve the dosimetric characteristics of Al_2O_3 by introducing oxygen vacancies into its structure; this was

accomplished by melting the material in a highly reducing environment where graphite was present. The resulting phosphor was found to be approximately 50 times more sensitive than LiF:Mg,Ti, with a minimum detectable dose of approximately 1 μGy (Akselrod *et al.*, 1990). The luminescence emission has been found to arise mainly from the F-centres, resulting in an emission peak centred at 420 nm (Akselrod and Kortov, 1990). It was discovered early on that α-Al_2O_3:C is highly sensitive to light, with a 10 min exposure to fluorescent light resulting in an 83% loss of TL signal (Moscovitch *et al.*, 1993). While this was initially perceived as a limitation of the material, its potential for use as a sensitive OSL dosimeter was quickly realized; in fact, experimental comparisons showed that the OSL sensitivity is 2 to 4 times greater than the TL sensitivity (Bøtter-Jensen and McKeever, 1996). Using pulsed OSL (POSL), Akselrod and McKeever (1999) arrived at a minimum measurable dose of 0.5 μGy, with the dose response remaining linear over nearly seven orders of magnitude. Unlike quartz, Al_2O_3:C displays a negligible sensitivity change over cycles of irradiation and heating, so it is possible to use a regeneration approach to dose assessment without the need for sensitivity correction (Bøtter-Jensen, 2000).

Other synthetic materials

A number of halides have been suggested as OSL phosphors, including KCl, KBr, NaCl, RbI, CaF_2, BaFX (X=Br, Cl, I) (Bøtter-Jensen *et al.*, 2003b). Eu-doped KCl and KBr have emission maxima at 420 nm, and both have been proposed for use in radiation dosimeters and in X-ray imaging phosphors. Analytical-quality and household NaCl have potential applications in dosimetry (Bailey *et al.*, 2000) and retrospective accident dosimetry (Thomsen *et al.*, 2002) respectively. Sulphates such as $MgSO_4$ and $CaSO_4$, compounds in the alkaline earth sulphide family (MgS, CaS, SrS and BaS), and oxides such as BeO and fused quartz have also been

suggested for use in OSL dosimetry (Bøtter-Jensen *et al.*, 2003b), but these will not be discussed here.

2.6 Instrumentation

The essential components of a system for the measurement of optically stimulated luminescence include a source of stimulation light, a light detection system (usually a photomultiplier tube), stimulation and detection filters, and readout electronics, as pictured in Figure 6.

2.6.1 Stimulation sources

The main stimulation sources in use are lasers, infra-red (IR) light emitting diodes (LEDs), IR laser diodes, broad-band light sources, green LEDs, and blue LEDs. The early OSL measurements on quartz carried out by Huntley *et al.* (1985) used the 514 nm line from an argon laser, and the single grain unit developed by Bøtter-Jensen *et al.* (2000) uses a Nd:YVO_4 laser. McKeever *et al.* (1996a) and Akselrod and McKeever (1999) have used Nd:YAG lasers at 532 nm for POSL dosimetry. Stimulation sources based on filtering green wavelengths from broad-band incandescent lamps were developed early on as a less expensive alternative to laser stimulation (Bøtter-Jensen and Duller, 1992).

The introduction of green-light and then shorter-wavelength blue-light LEDs offered a number of advantages over other stimulation methods. LEDs are small and inexpensive, and they can switch on and off quickly, with no warm-up period required. They also provide the possibility of software-controlled light intensity for linearly-modulated OSL (LM-OSL) measurements. The blue LEDs now commonly in use have a peak emission wavelength at 470 nm with a 20 nm full width at half maximum (FWHM). In the Risø automated TL/OSL reader, these are arranged in clusters of seven LEDs, with up to seven clusters mounted in a ring surrounding the sample

position at a distance of about 30 mm. A focused IR laser diode (for feldspar measurements) often occupies one cluster position (Bøtter-Jensen *et al.*, 2003b).

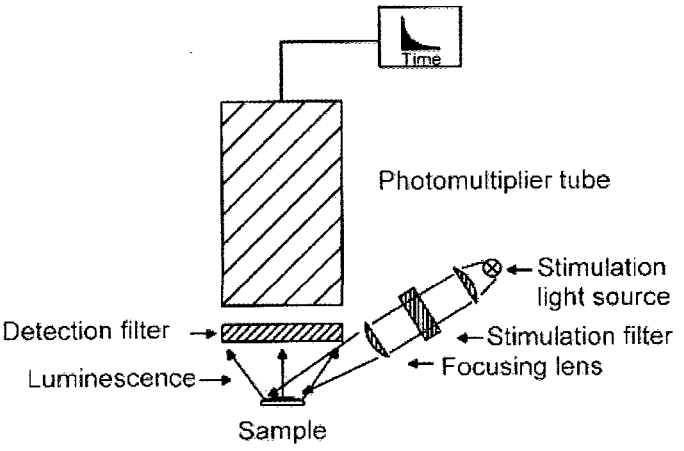

Figure 6. Basic components of an OSL detection system (Bøtter-Jensen *et al.*, 2003b)

2.6.2 Light detection

Photomultiplier tubes (or PM tubes) are both the most sensitive and most ubiquitous type of light detectors (Bøtter-Jensen *et al.*, 2003b). A PM tube invariably consists of a vacuum tube with a photosensitive cathode, a series of dynodes for multiplying electrons emitted from the photocathode, and an anode held at high voltage (normally 1000 V) (Bøtter-Jensen, 1997). When photons hit the cathode (often potassium-caesium), electrons are emitted and attracted to the positive voltage of each dynode in turn. Since two or three electrons are emitted for each electron hitting a dynode, a single photon is observed as millions of electrons reaching the anode. A photomultiplier tube's sensitivity varies with wavelength, and only up to 25% of photons result in the detection of electrical pulses at the anode. Typically, a bialkali PM tube detects photons most effectively at a wavelength of approximately 400 nm, but some are designed to have increased sensitivity in the red region, although these normally require cooling. Dark currents of modern bialkali tubes can be well below 20 cps at room temperature, with the count

rate decreasing with cathode area; small diameter (10 mm) tubes therefore provide a better signal-noise ratio (Bøtter-Jensen *et al.*, 2003b)

2.6.3 Automated OSL readers

The requirement to perform regenerative-dose procedures on large numbers of samples created a need for computer-controlled equipment able to perform automated OSL measurements, as well as heat and irradiate samples. Bøtter-Jensen (1997, 2000), Bøtter-Jensen *et al.* (2000, 2002), and Bortolot (1997, 2000) describe the development of such readers, and a detailed description of the Risø TL/OSL system is given in Section 3.2. For regenerative-dose measurements such as those described in Section 2.4.2, an integrated, automatic beta irradiator is necessary. A $^{90}Sr/^{90}Y$ beta source is typically used, with a 1.5 GBq (40 mCi) $^{90}Sr/^{90}Y$ source giving a dose rate of ~0.1 Gy/s at the sample in a Risø TL/OSL reader (Bøtter-Jensen *et al.*, 2003b). In addition to automated irradiation, OSL readers must also be able to accurately heat samples at heating rates from 0.1-30°C/s and carry out OSL measurements at elevated, constant temperatures (Bøtter-Jensen *et al.*, 2000). Temperatures above 500°C are not generally necessary for measurements involving minerals such as quartz and feldspar, but the ability to heat samples above 700°C may be useful for specialized applications, such as the study of deep trapping states (Bøtter-Jensen *et al.*, 2003b).

It is also possible to install a heating strip under the irradiation position of the reader, as reported by Bøtter-Jensen *et al.* (2000), allowing for irradiation of samples at elevated temperature. They found that introducing the ability to hold samples at temperatures of up to 200°C during irradiation, in order to keep the shallow traps empty, allowed the influence of competition from these traps, a possible source of dose-rate dependence of luminescence response, to be studied in detail (Bøtter-Jensen *et al.*, 2000). In addition, an attachment has been developed to allow the

observation of radioluminescence (RL), using a light guide to direct the luminescence emitted during irradiation to the PM tube (Bøtter-Jensen *et al.*, 2003a). This can be used, in combination with the added heating strip, to allow the observation of RL at elevated temperature.

CHAPTER 3: MATERIALS AND METHODS

3.1 Materials

Electronic components, such as resistors, capacitors, and resonators, all include a dielectric substrate (usually ceramic) in their construction. The use of porcelain and other ceramics in retrospective dosimetry is well-established; household items, such as porcelain dishes and bathroom fixtures, were used extensively for estimating population doses following Chernobyl (Bailiff, 1995). The goal of the research reported in this thesis has been to study a range of materials found in personal electronic devices such as cellular phones, digital watches, and personal media players, in order to identify components displaying an OSL response following irradiation.

Components for analysis were obtained from a number of sources, including samples of several models of surface-mount resistors, capacitors, and inductors manufactured by Cal-Chip Electronics. Detailed information on the construction of these components and the composition of the substrates was available on the Cal-Chip Electronics website (Cal-Chip Electronics, 2007). Figure 7 illustrates the components of a typical surface-mount resistor. Samples were packaged in strips cut from tapes, normally affixed to reels for automatic placement, as pictured in Figure 10.

In this case, the substrate, which accounts for 89.1% of the total weight of the resistor, is composed of 97.03% aluminum oxide (undoped) and 2.9% silicon dioxide. Capacitor substrates were listed as consisting primarily of $BaTiO_3$, $CaTiO_3$, or $Ca/MgTiO_3$. While the OSL

properties of titanates are not well known, aluminum oxide (in a carbon-doped form as TLD-500) has superior dosimetric properties.

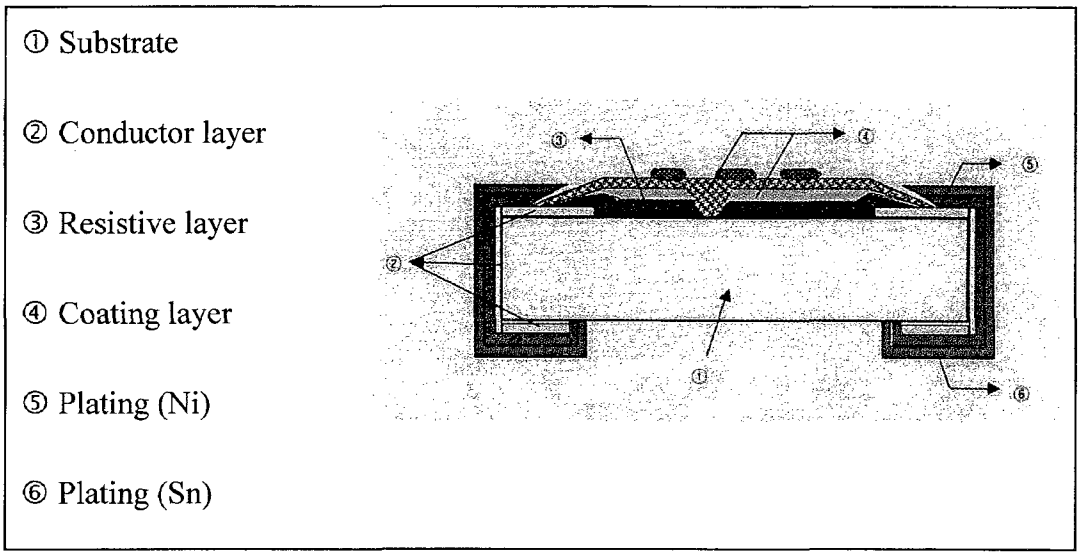

Figure 7. Diagram of a Cal-Chip RM06 series surface mount resistor.

In addition, Research In Motion (RIM) supplied several Blackberry™ smartphones for study; Figure 8 shows one of the Blackberry circuit boards. Further, a number of cellular phones (as in Figure 9) were used in early experiments. Once this limited supply was exhausted, a large number of broken cellular phones from various manufacturers were graciously supplied by a local repair shop (Cellphone Rescue).

Table 2 lists specific models of phones used in these experiments. Cellular phones were disassembled using precision screwdrivers, and the circuit boards were extracted. Individual components were removed from the circuit board using a sharp utility knife – effectively a brute force method. Unfortunately, other more elegant methods, such as applying heat to melt the solder securing the components to the circuit board, would have compromised the heat-sensitive OSL signal.

Table 2. Cellular phones used in experiments.

Manufacturer	Models
Motorola	120c, StarTAC
Nokia	3360, 6185
Panasonic	EB-TX310CST
Samsung	SCH-N370, SCH-3500SPH-A460, SPH-A660, SPH-T100

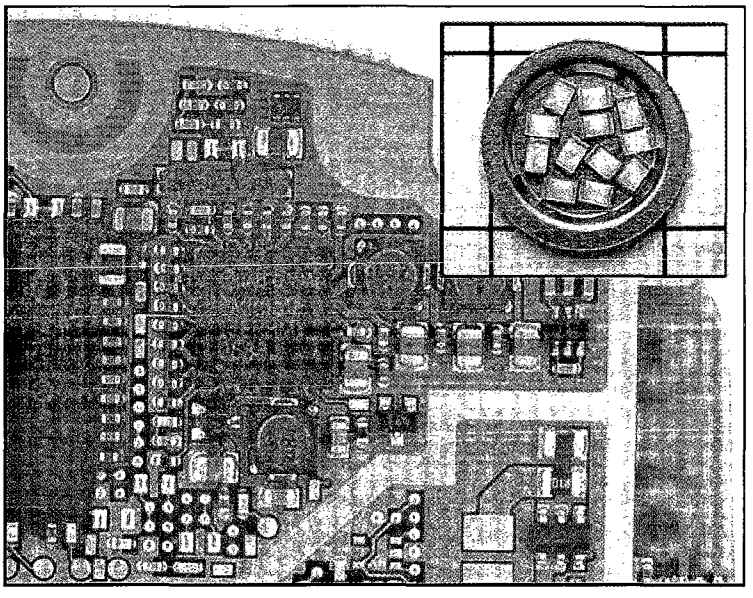

Figure 8. Section of a circuit board from a RIM Blackberry. Inset: resistor sample prepared for analysis, displayed on a 1 cm grid.

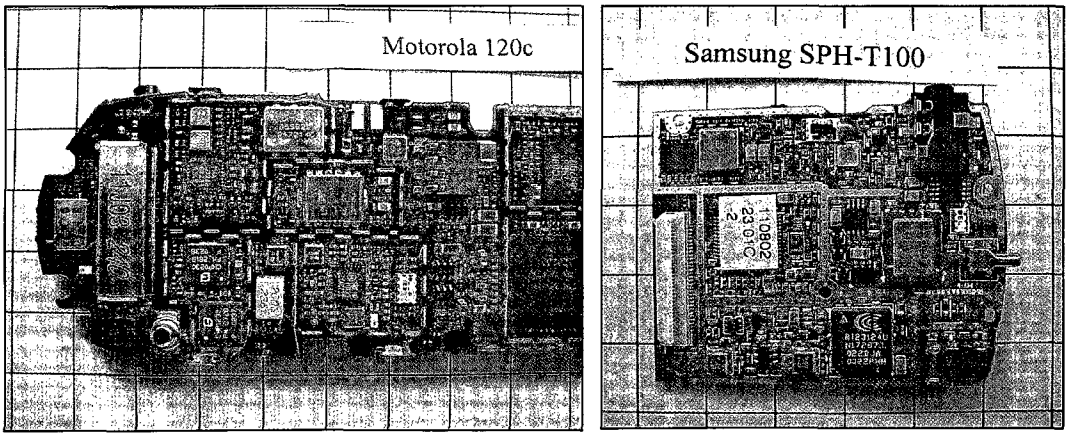

Figure 9. Circuit boards of cellular phones used for initial experiments.

For the later signal fading experiments, a larger quantity of new resistors was required to allow experiments to be conducted with standard materials. This ensured repeatable results and allowed sufficient numbers of samples to be analysed to ensure statistical significance. Three models of resistors manufactured by Bourns, Inc. and packaged as in Figure 10, were obtained for this purpose.

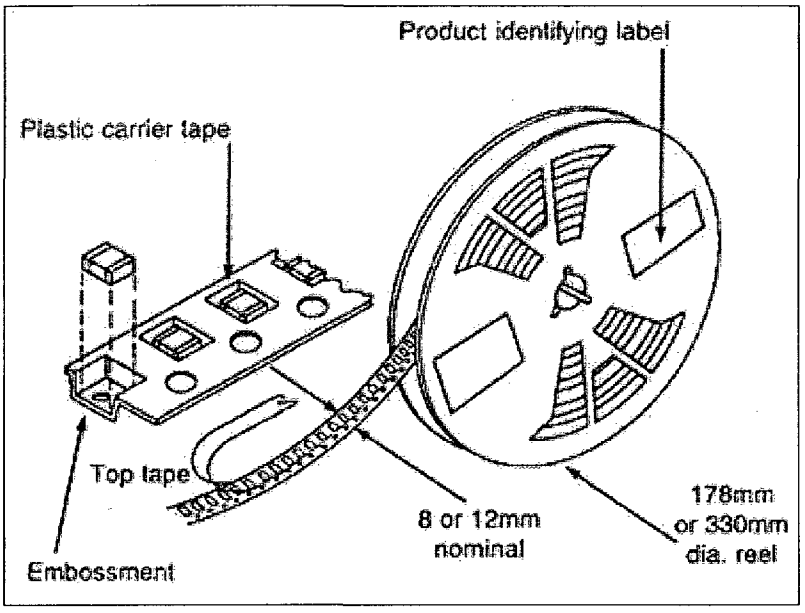

Figure 10. Packaging of surface-mount component samples (Cal-Chip Electronics).

Samples were prepared for analysis by coating an aluminum planchette (10 mm in diameter) with a thin layer of silicon oil and arranging a number of resistors, bare substrate side up, on the surface (as in Figure 8, inset). The bottom surface of components removed from circuit boards were observed to be coated with an epoxy residue, a result of the manufacturing process, in which components are first affixed to the circuit board with an adhesive before being soldered into position. Figure 11 shows resistors removed from a Nokia 6185 circuit board, before and after soaking them in dichloromethane for approximately 30 minutes to remove the adhesive.

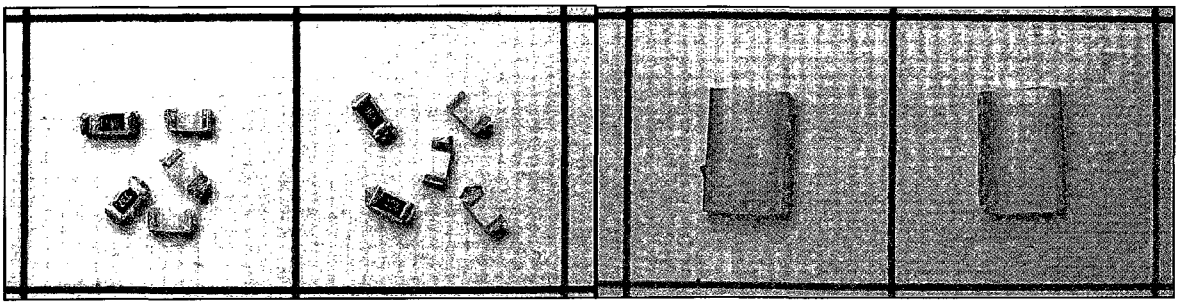

Figure 11. Resistors (left) and a resistor array (right), before and after removal of epoxy residue.

3.2 Instrumentation and equipment

All experiments were carried out using a Risø TL/OSL-DA-15 automated TL and OSL system, pictured in Figure 12 as set up in the DRDC Ottawa OSL laboratory (Risø DTU, 2008). The primary components, which are described in detail below, are the luminescence stimulation system, the light detection system, and the irradiation source. Figure 13 illustrates the overall configuration of the system.

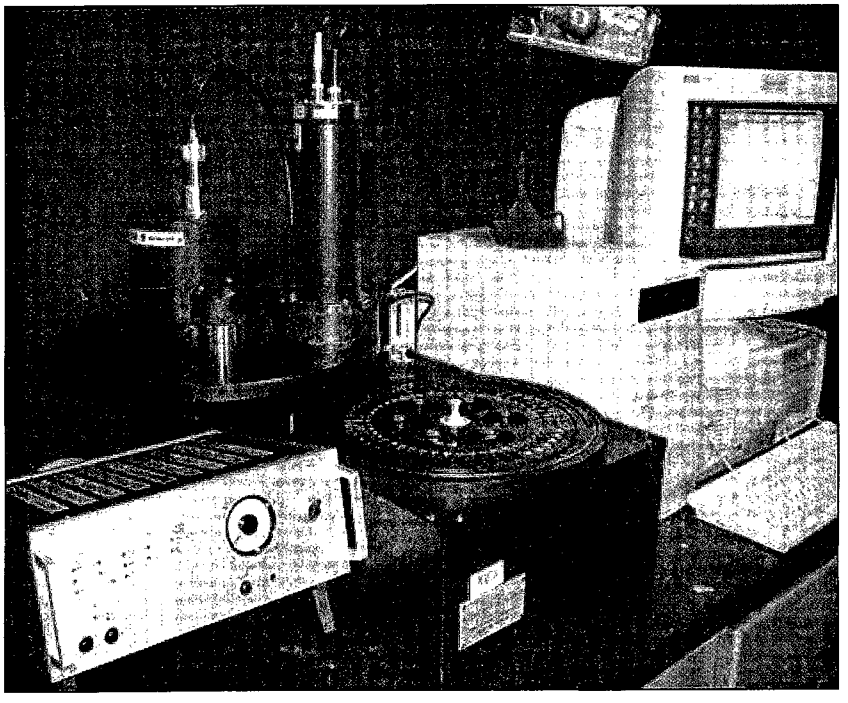

Figure 12. Risø TL/OSL-DA-15 system in DRDC Ottawa OSL laboratory.

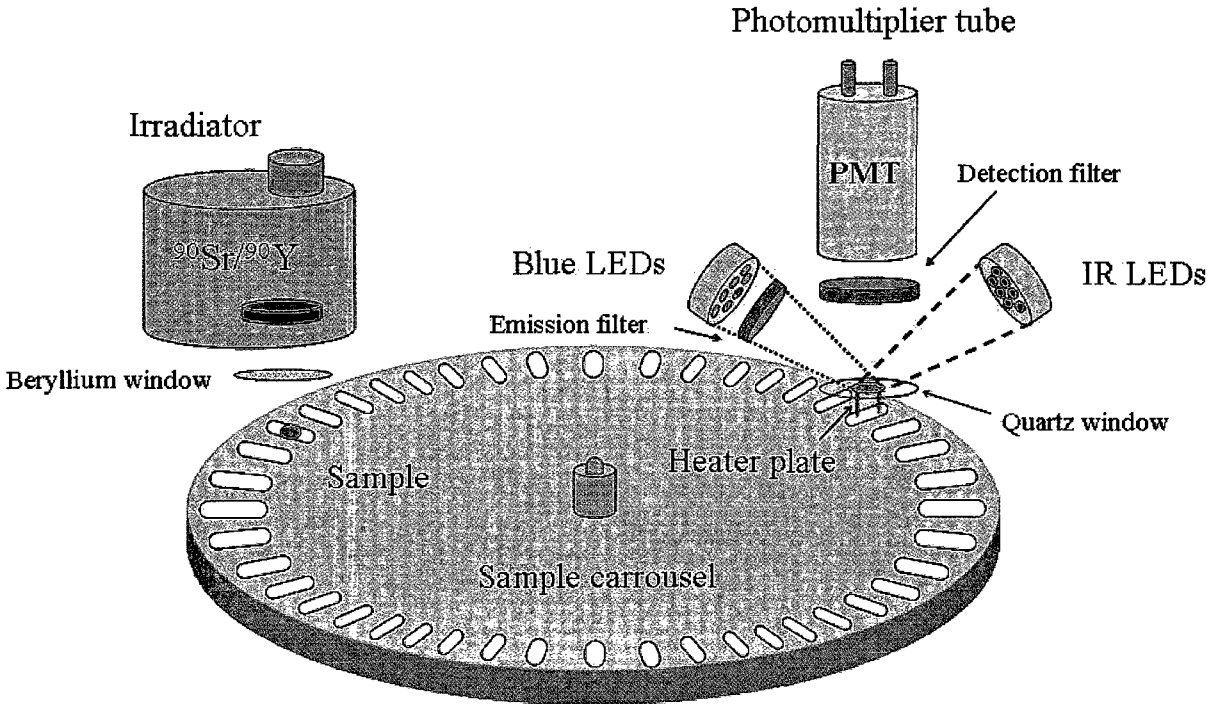

Figure 13. Schematic diagram illustrating the components of the Risø TL/OSL reader (Risø DTU, 2008).

The OSL system is connected to the TL/OSL-DA-15 control box (silver instrument on left of Figure 12), which in turn is connected to the *Minisys*, a 486-based PC which is connected to the user PC by an RS-232 serial cable. Two software programs installed on the user PC, *Control* and *Sequence Editor*, allow the user to send individual commands to the system (via *Control*) or to program the system to carry out a user-defined sequence of operations (via *Sequence Editor*).

The motorized carrousel may receive up to 48 samples loaded into 10 mm aluminum sample cups or affixed to 9.7 mm steel discs. Once closed, the sample chamber can be flushed with nitrogen as needed in order to permit heating to high temperatures without sample oxidation; as a rule, this is done when heating to 200°C or above.

3.2.1 Luminescence stimulation system

Thermal stimulation system

The luminescence stimulation system of the TL/OSL-DA-15 includes both a heating system for TL measurements and an optical stimulation system for OSL measurements. The heating system can also be used to carry out OSL measurements at elevated temperatures. This is often desirable as it can improve luminescence efficiency by preventing the re-trapping of electrons in low-temperature TL traps. The combined heating system and lift mechanism, pictured in Figure 14, is located below the PMT. The heating element is made of a high-resistance alloy known as Kanthal, and is designed to keep the sample from moving and to provide optimal surface contact with the sample tray, ensuring a reproducible measurement position and even heat transmission. When samples are heated, a controlled current is passed through the heating element, and the temperature is monitored with a Cromel-Alumel thermocouple affixed to the bottom of the heater strip. The system is capable of heating samples at constant rates of 0.1 to 10 °C $\cdot s^{-1}$ to a maximum temperature of 700°C , and a software-based calibration is applied to correct for systematic nonlinearity in the heating rate (Risø DTU, 2008).

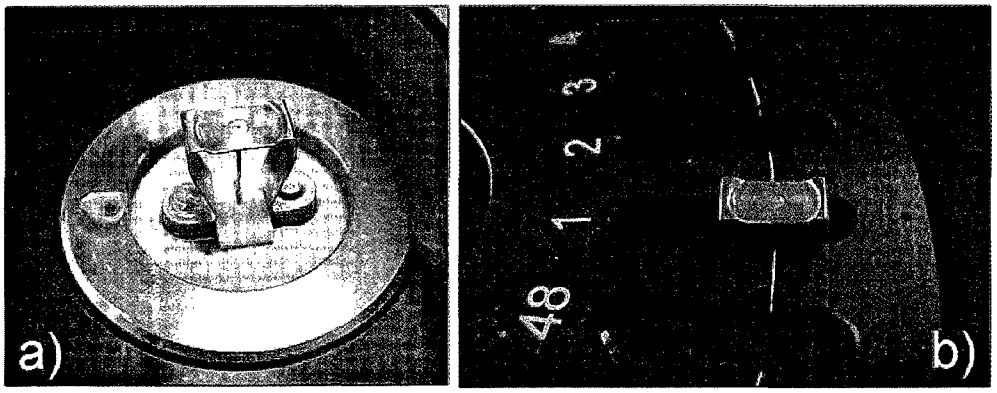

Figure 14. Picture of the heating element of the Riso TL/OSL reader without (a) and with (b) the carousel in place (Risø DTU, 2008).

Optical stimulation system

Figure 15 shows the configuration of the optical stimulation system, which is capable of providing stimulation in the blue (470 nm, FWHM = 20 nm) and the infrared (870 nm), although only blue stimulation was used in these experiments. Blue light of intensity up to 50 mW/cm^2 is delivered at the sample location (approximately 20 mm from the diodes) by 28 blue LEDs arranged in four clusters. A green long pass filter (GG-420) installed in front of the blue LEDs attenuates the high-energy tail of the LED emissions, minimizing the scattered light entering the detection system (Risø DTU, 2008). These experiments consistently used illumination with blue LEDs at 90% of maximum intensity, as this prolongs the life of the LEDs (relative to full-intensity illumination) (Risø DTU, 2008).

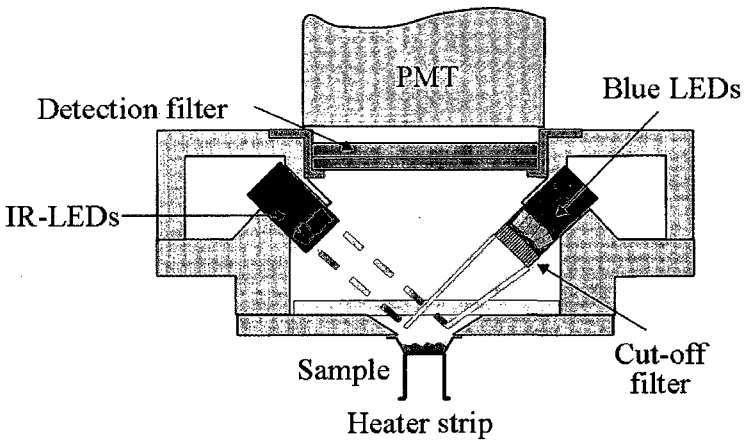

Figure 15. Diagram of the Risø OSL unit (Risø DTU, 2008).

3.2.2 Light detection system

The light detection system consists simply of a photomultiplier tube (PMT) and removable detection filters installed between the sample and the PMT. The cathode of the PMT is coated with a photo-emissive bialkali compound which typically converts ten visible photons into one to

three electrons (Risø DTU, 2008). The maximum detection efficiency of the PMT installed in the TL/OSL-DA-15 (model EMI 9235QBF) is obtained in the 200 to 400 nm range, as illustrated in Figure 16.

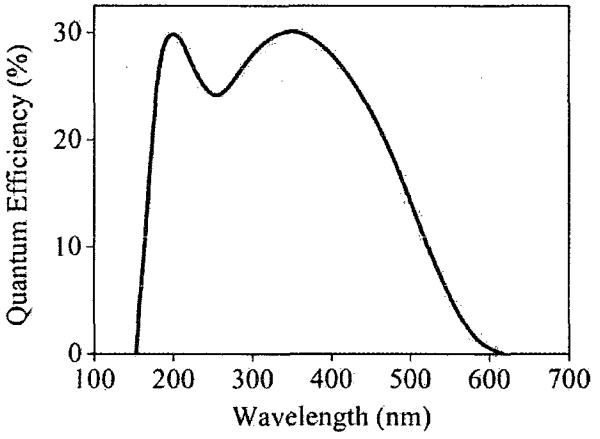

Figure 16. Quantum efficiency of the bialkali PMT (EMI 9235QB) as a function of wavelength (Risø DTU, 2008).

The intensity of the stimulation light is approximately 18 orders of magnitude greater than the luminescence emitted from most samples; hence, the use of proper detection filters is crucial to prevent stimulation light from overwhelming the luminescence signal reaching the PMT (Bøtter-Jensen *et al.*, 2003b). For this reason, a Hoya U-340 filter is installed in the detection system; the transmission curve, pictured in Figure 17, has a maximum at 340 nm. This is suitable for the measurement of emissions from aluminum oxide-based ceramics, which are expected to have similar emission characteristics to Al_2O_3:C, namely a broad emission peak centred at 420 nm.

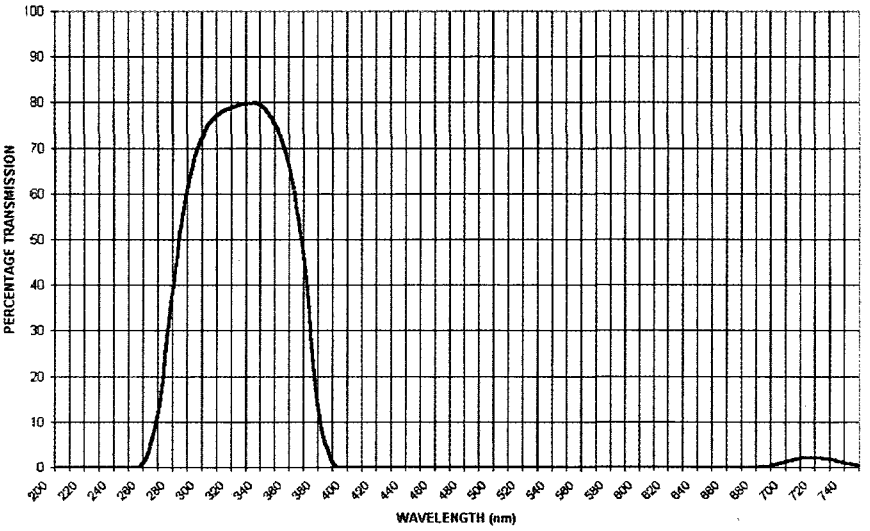

Figure 17. Transmission curve of the Hoya U-340 optical filter.

3.2.3 Irradiation source

Source characteristics and configuration

Except where indicated otherwise, all samples were irradiated with the integrated 1.48 GBq (40 mCi) $^{90}Sr/^{90}Y$ irradiator, pictured in Figure 18. The $^{90}Sr/^{90}Y$ source emits beta particles, with an E_{max} of 2.27 MeV for ^{90}Y, and its 30-year half-life means that minimal correction for radioactive decay is required, particularly as it is regularly calibrated against a reference ^{60}Co gamma source. The beta source is mounted on a pneumatically-activated rotating stainless steel wheel, so that when the source is off, it is pointing directly at the 10 mm carbon absorber, and when it is on, it points downward towards the irradiation position (Risø DTU, 2008). As samples are closely-spaced on the carrousel, the issue of irradiation cross-talk has been considered. Markey *et al.* (1997) experimentally quantified the cross-talk as 0.250 ± 0.003% for the nearest samples and 0.014 ± 0.002% for the second nearest samples; in most cases, this can be considered negligible. Bray *et al.* (2002) reported a lower level of cross-irradiation, at 0.006% for the nearest sample, but additionally measured cross-illumination of 0.014%, resulting in a reduction of the signal from the adjacent sample by as much as 20%, depending on the measurement protocol used.

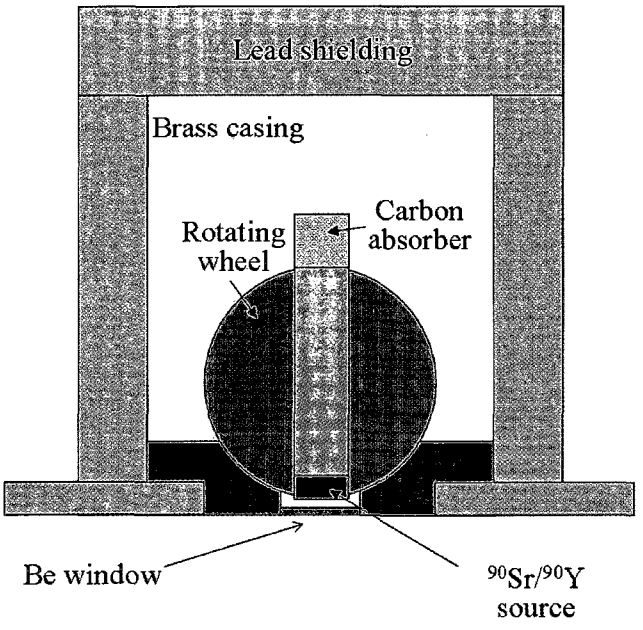

Figure 18. Cross-section of the Risø beta irradiator (Risø DTU, 2008).

Beta source calibration

The beta source is calibrated by performing a SAR measurement protocol on standard, high-purity quartz, supplied by the Risø laboratory, which has been irradiated to a known dose with a reference gamma source. The measurement protocol used is identical to that described in Table 1, with a 260°C preheat used for the regeneration doses, and a 220°C preheat for the test doses. The regeneration doses are chosen (based on an estimate of the dose rate) in order to bracket the nominal quartz dose.

Based on the calibrations performed, the beta irradiator in the DRDC Ottawa TL/OSL reader delivers a dose rate (in quartz) of 0.102 $Gy \cdot s^{-1}$ at the sample site. When a removable 2.2 mm aluminum attenuator is placed between the source and the irradiation position, the dose rate is reduced to 4.5 $mGy \cdot s^{-1}$ (in quartz). It should be noted that, with the exception of the RED trial

results, the doses reported in this work are effectively doses in quartz, as this is the basis for the beta source calibration.

3.3 OSL and TL measurement procedures

3.3.1 OSL curve analysis

Identification of sensitive components

In order to identify which electronic components produced an OSL signal following irradiation, a large number of components were given doses from 0.045–0.45 Gy (10-100 s irradiations with the aluminum attenuator installed). This dose range was selected in order to limit the investigation to those components capable of detecting a dose of ~0.5 Gy or less. Following irradiation, the OSL emission of each sample was measured for 40 s at room temperature, without preheating. The samples studied included resistors, capacitors, resonators, and some unidentified components removed from the Blackberrys and cellular phones, as well as resistors, capacitors, inductors, and ferrite beads from the Cal-Chip samples. Of these components, surface-mount resistors were selected as the focus for further study, based on the consistent observation of a measurable OSL response (see Section 4.1 for details).

Measurement of net OSL signal and limit of detection

The OSL signal was typically measured for 40 s, with 10 data points collected per second (at 0.1 s intervals). In some cases, the measurement was started one second before illumination began, in order to observe the dark current of the PMT. Figure 19 is an illustration of a typical OSL curve. The first 10 channels (1 s) of the OSL curve were integrated to give the gross OSL signal. Subtraction of the background based on the last 50 channels (which may include dose-independent photoluminescence and hard-to-bleach slow OSL signals) gave the net OSL signal.

An advantage of using only the first part of the OSL curve for analysis is that it provides the greatest signal to noise ratio.

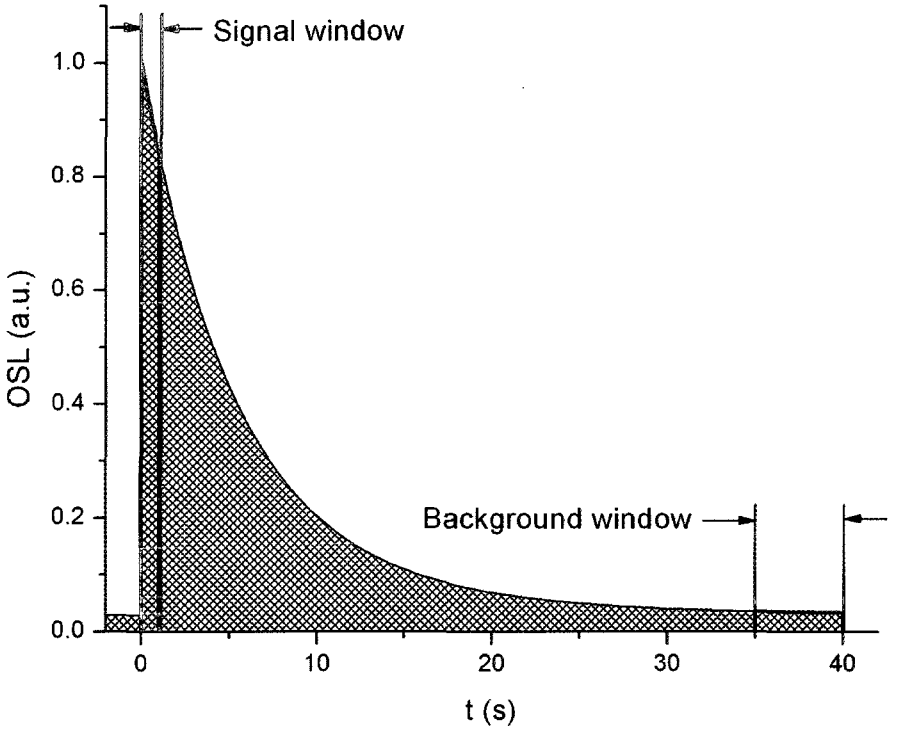

Figure 19. Selection of signal and background windows for OSL analysis.

The uncertainty of the OSL signal is governed by counting statistics, meaning that if M counts are observed in the signal window, the standard deviation is $\sqrt{M}$, so the gross OSL counts can be expressed as $M \pm \sqrt{M}$. Taking into account the background, B, the net OSL signal, N, is given by $N = M - B$, and the uncertainty on the net signal is therefore given by $\sqrt{M+B} = \sqrt{N+2B}$. To report the presence of an OSL signal at the 95% confidence level (2 standard deviations), the requirement is thus

$$N > 2\sqrt{N+2B} \tag{19}$$

It is also important to consider the limit of quantitation, or the minimum level at which a signal can be reported with a given level of certainty. Define $S = \frac{M}{B}$, essentially the signal to background ratio. At the 95% confidence level, the relative uncertainty on the net signal is

$$\frac{2\sqrt{N+2B}}{N} = 2\sqrt{\frac{S+1}{B(S-1)^2}} \tag{20}$$

Equation 20 can thus be used to estimate the uncertainty of a given net OSL measurement, or to approximate the gross OSL signal required to achieve a given level of uncertainty (based on an estimate of the background). It should be noted that only uncertainties related to counting statistics are considered here.

3.3.2 TL properties

Thermoluminescence glow curves of resistor substrates were measured using a sequence of irradiation to 2.25 Gy (with the aluminum attenuator installed) followed by heating to $500°C$ at a rate of $5°C \cdot s^{-1}$. Fitting was performed using GlowFit, a TL glow curve deconvolution software program. The user is required to select the number of peaks for fitting as well as the initial values for the maximum temperature, intensity, and energy of each peak. GlowFit then displays the best fit and writes the associated parameters to a file. The fit parameters for each peak may also be adjusted manually. The quality of the fit can be evaluated visually by examining the plot of residuals displayed on the screen. A parameter describing the quality of fit, the figure of merit (FOM) is also calculated as follows:

$$FOM[\%] = \frac{\sum_i |y_i - y(x_i)|}{\sum_i y_i} \times 100\% \tag{21}$$

where y_i is the TL signal of channel i, and $y(x_i)$ is the value of the fitting function at channel i (Puchalska and Bilski, 2006); a lower FOM is thus indicative of a better fit. In addition to the FOM, the GlowFit program calculates a value of s, the "attempt-to-escape" frequency, for each peak. In theory, this parameter, along with the peak energy and temperature, allow the half-life for thermal fading to be calculated as follows (Bos, 2001):

$$t_{1/2} = \frac{\ln 2}{s \exp(-E/kT)} \tag{22}$$

In order to explore the relationship between the TL curve and the OSL emission from alumina substrates, TL measurements were taken following various durations of exposure to blue light from the LEDs. A set of six Cal-Chip 68.1Ω resistors (RM10F68R1CT) was subjected to repeated cycles of irradiation to 2.5 Gy, preheating to 130°C (to eliminate the thermally unstable signal), illumination for times varying from 0 – 3000 s, and TL measurement to 500°C (at 5°C·s^{-1}).

3.3.3 Selection of preheat and measurement temperatures

The preheat temperature was selected based on the shape of the TL curve; that is, it was selected such that all luminescence expected to be thermally unstable at room temperature (according to Equation 22) would be eliminated before the OSL measurement was performed. This is done in order to simulate a period of storage at room temperature following irradiation, as would be the case for a dosimetric sample. For most experiments, samples were heated to 120°C – 130°C, held at this temperature for 10 s, and cooled to 60°C before the OSL measurement was performed. In some experiments, other preheat temperatures were used in order to examine the effect of varying the preheat temperature on the signal fading rate.

To study the effect of the sample temperature during OSL measurement, one Cal-Chip 68 Ω resistor was repeatedly irradiated to 0.45 Gy and preheated to 130°C before the OSL signal was measured at temperatures ranging from room temperature (~20°C) to 120°C. The sample was heated to 500°C between measurements in order to zero the signal. Based on the results of these measurements (described in the next chapter), OSL measurement for subsequent experiments was carried out at 90°C.

3.3.4 Dose response curves and variability of OSL response

Experiments were carried out to construct dose response curves for a number of resistor types, including Cal-Chip resistor samples and components removed from cellular phones. The typical measurement sequence consisted of repeated cycles of irradiation, preheating (120°C 120°C), and OSL measurement (90°C 90°C) following irradiation to doses ranging from 0.0045 Gy to 4.5 Gy (with attenuator installed). The response at high doses was studied by removing the attenuator and repeating this sequence for a single Cal-Chip 68 Ω resistor irradiated with doses up to 98 Gy.

To obtain an indication of the consistency of the OSL response, 6 models of resistor were selected from the Cal-Chip RM10 series. Six different samples were prepared, each consisting of three resistors of the same type. The background OSL signal for each sample was measured for 40 s at 90°C 90°C, after which each sample was heated to 500°C 500°C to remove any residual signal. Four cycles of irradiation to 0.45 Gy (with attenuator installed), preheating to 120°C 120°C, 40 s blue OSL at 90°C, and heating to 500°C 500°C were carried out for each sample.

3.4 OSL signal fading studies

3.4.1 Short-term fading experiments

Short-term fading experiments were conducted on multi-resistor aliquots of chip resistors manufactured by Bourns, Inc. (CR0805-FX-1200E). Measurement sequences were developed to incorporate automated delays of 30 s to 8.4 h between beta irradiation and OSL measurement. In order to account for greater depletion of the OSL signal with higher preheat temperatures, the doses were varied: 0.45 Gy for 120°C , 135°C 135°C, and 150°C 150°C preheats, 2 Gy for the 160°C 160°C preheat, and 10 Gy for the 200°C 200°C and 260°C 260° preheats. The OSL response was normalized to the response from a 0.43 Gy test dose administered using the integrated $^{90}Sr/^{90}Y$ source.

For the 120°C 120°C to 150°C 150°C preheats, only one aliquot (of 10 resistors) was analysed for each preheat temperature, while for the three higher-temperature preheats 12 aliquots of 10 resistors were analysed for each preheat temperature, and the average of these measurements was used in the analysis. Delay times were calculated from the difference between the system time at the beginning of each OSL measurement and the time at the midpoint of the previous irradiation, in order to take into account fading during irradiation.

3.4.2 Long-term fading experiments

Two experiments were carried out to study the long-term fading behaviour of the OSL signal (meaning days to months vs. hours), one using Cal-Chip resistor arrays (P/N CN34J681CT, CN34J101CT) and another with Bourns Inc. resistors (P/N CR0805-FX-1200E). In both cases, a large number of components were placed in light-tight vials and secured between two buildup layers consisting of 5 mm sheets of plexiglass (to ensure electrostatic equilibrium), then

irradiated to approximately 5 Gy using a GB-150C ^{60}Co irradiator (dose rate 18.02 Gy/h at 1 m). The Cal-Chip resistor arrays were measured individually following delays from 1 h to 20 weeks. OSL from the 680 Ω resistor arrays was measured for 40 s at room temperature, while the 100 Ω arrays were preheated to 120°C prior to measurement for 40 s at 90°C. To provide a reference response, both were then irradiated to 5 Gy, preheated to 120°C, and measured at 90°C for 40 s. The fading rate was then determined by plotting the ratio of the first measurement to the reference measurement versus the time since irradiation. The Bourns resistors were analysed in the same manner, with the exception that a preheat and elevated temperature measurement were always used.

3.4.3 Fading corrections

Fading corrections were applied following the method proposed by Huntley and Lamothe (2001), described in Section 2.4.4. The intensity at time t following irradiation is then given by Equation 18.

The value of g depends on the choice of t_c, and the approximations used in deriving Equation 18 are not valid for small values of t. When the OSL intensity is plotted against $\log(t / t_c)$, the value of g can easily be calculated from the slope and intercept of a linear fit to the resulting curve. In cases where the duration of the irradiation was not negligible in comparison to the time between irradiation and analysis, Equation 18 was integrated over the irradiation period to account for fading during irradiation. Detailed derivations are provided in Appendix A.

3.5 Experimental setup for RED simulations

Two trials were conducted, in which cellular phones were affixed to a Humanoid RT-200 anthropomorphic phantom at belt level and exposed to a radioactive source in a geometry

designed to simulate the deployment of an RED under a park bench or a desk. An MGP SOR/R electronic dosimeter (ED) was affixed to each device to record an approximate dose, and an additional ED was placed mid-gut inside the phantom. In Trial 1, three cellular phones were exposed to a 1.1 GBq (30 mCi) ^{60}Co source for approximately 3.5 d, while Trial 2 exposed four devices to a 74 GBq (2 Ci) ^{137}Cs source for 4 h; in each case, the distances between the source and the devices were in the range of 25–40 cm.

In preparation for analysis, each device was disassembled under darkroom conditions and the resistors were removed from the circuit boards using a utility knife. The resistors were then soaked in dimethylchloride for approximately 30 min in order to remove any adhesive from the bottom of each component. Each planchette was coated with a thin layer of silicone oil to keep the resistors in position. Resistors were then arranged bottom-up on the planchettes, with as many components as would fit placed on a single planchette. In general, each device yielded enough resistors for one to two samples.

Table 3 gives details of the analysis procedure. For each sample, the OSL response to the trial dose was measured along with the response to four regeneration doses, each of which was followed by a 45 mGy test dose. The first regeneration dose was repeated as a check for sensitivity change. The OSL response was then plotted against regeneration dose, and the accident dose determined by interpolation. The three cellular phones from Trial 1 were analysed at different times following the experiment (4 - 18 days), while those from Trial 2 were all analyzed 21 days after irradiation.

Table 3. SAR measurement sequence for simulated RED experiments.

Step	Regeneration dose (Gy)	Measurement	Test dose (Gy)	Measurement
1	N = Accident dose	Preheat (120°C) 100 s OSL (90°C) TL to 250°C	$T_0 = 0.045$	Preheat (120°C) 100 s OSL (90°C) TL to 250°C
2	$R_1 = 0.22$		$T_1 = 0.045$	
3	$R_2 = 0.45$		$T_2 = 0.045$	
4	$R_3 = 0.68$		$T_3 = 0.045$	
5	$R_4 = 0.90$		$T_4 = 0.045$	
6	$R_5 = R_1 = 0.22$		$T_5 = 0.045$	

Figure 20. Cellular phones and electronic dosimeters affixed to DRDC Ottawa's anthropomorphic phantom for RED simulation trials.

CHAPTER 4:

RESULTS AND DISCUSSION – OSL AND TL CHARACTERISTICS OF ELECTRONIC COMPONENTS

4.1 Sensitivity and OSL response

Initial experiments demonstrated that surface-mount resistor alumina substrates consistently exhibited OSL following irradiation. Dark-coloured barium titanate and calcium titanate components, such as capacitors and inductors, gave little or no OSL response to the range of doses administered. Figure 21 shows a typical OSL curve, fit with a stretched exponential function, as described by Equation 14 (in Section 2.3.2), with the addition of a constant to represent the background signal. Room-temperature OSL curves for 6 varieties of Cal-Chip resistors irradiated to 0.14 Gy are shown in Figure 22. The samples analysed in this experiment are described in Table 4. All of the surface-mount resistors tested produced OSL signals, although the intensity of these signals varied significantly. All OSL signals displayed a rapid initial decay, followed by a slow decay at a much lower signal level. None of the capacitors or inductors tested produced OSL.

The experiment was repeated using components extracted from three cellular phones irradiated to 0.45 Gy; the sample details are provided in Table 5, and the resulting OSL curves are shown in Figure 23. As with the Cal-Chip samples, all resistors produced OSL signals, and capacitors and inductors did not; however, a resonator, which appeared to have a white ceramic substrate, did produce a signal. Following the initial OSL measurement, the samples were heated to 500°C to remove any residual signal, and the measurement was repeated, incorporating a preheat to

120°C. Surprisingly, when the sequence of irradiation and measurement was repeated, OSL was only observed from some of the resistor samples. The measurement was repeated with no preheat, and once again, OSL was only observed from some samples, and at greatly reduced intensity (see Table 5). Upon inspection, the surfaces of these resistor substrates were no longer white, but appeared blackened.

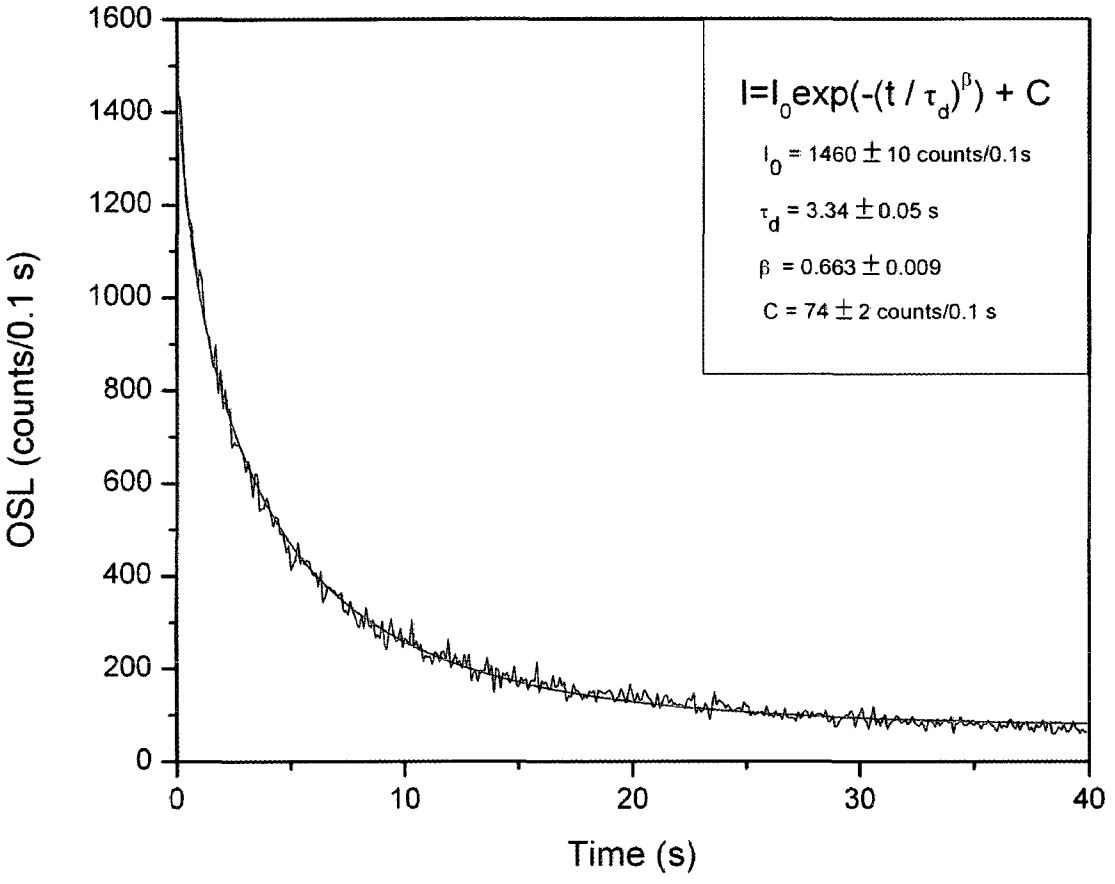

Figure 21. OSL curve of a resistor sample irradiated to 4.5 Gy, fitted with a stretched exponential ($R^2 = 0.99$)

Table 4. OSL response at room temperature of Cal-Chip components irradiated to 0.14 Gy (no preheat).

Position	Component	Mass (mg)	Net OSL* (a.u.)
1	470 Ω	4.7	311
2	1 kΩ	2.1	180
3	1 MΩ	2.2	50
4	22 kΩ	2.3	74
5	68.1 kΩ	5.0	507
6	100 Ω	8.7	881
7	0.1 μF (x 3)	4.2	0
8	150 pF	4.7	0
9	2200 pF	7.8	0
10	1 pF	3.7	9
11	inductor	4.8	0
12	inductor	13.3	4
13	ferrite bead	11.5	0

*Note: Negative numbers are reported as 0.

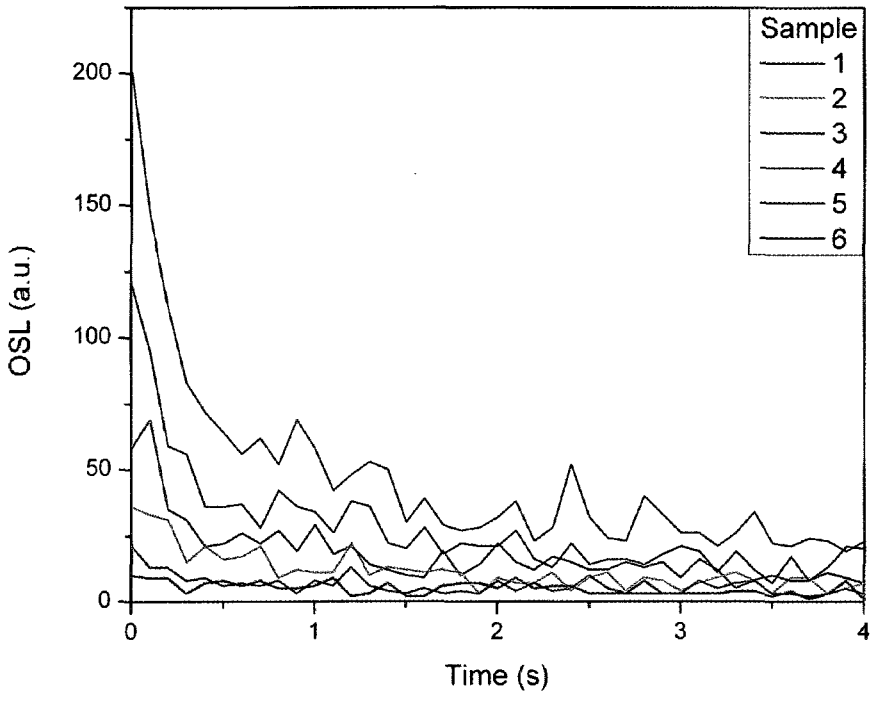

Figure 22. OSL curves for Cal-Chip components irradiated to 0. 14 Gy (see Table 4 for sample details).

Table 5. OSL response at room temperature of cellular phone components irradiated to 0.45 Gy (no preheat).

Model	Sample	Type	Mass (mg)	Net OSL (a.u.)	
				Initial Measurement	Repeated Measurement
Blackberry	10	resistors	8.2	587	6
	11	resistor arrays	34.5	951	37
Motorola 120C	12	resonator	104.6	84	6
	13	resonator	9.3	0	–
	14	resistor	10.2	661	30
	15	capacitor	90.7	0	–
	16	inductor	11.4	210	16
	17	resistors	3.9	822	150
Samsung A660	18	resistor	9.9	304	0
	19	resistors	10.8	416	37
	20	unknown	7.8	1	–
	21	resonator	18.3	10	–
	22	unknown	6.5	4	–
	23	capacitors	124.3	0	–
	24	capacitors	6.7	6	–
	25	capacitors	19.6	8	–

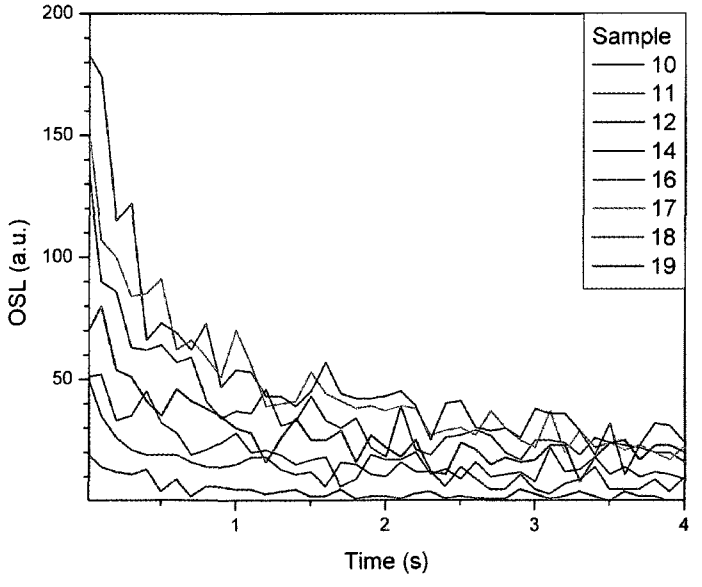

Figure 23. OSL curves for cellular phone components irradiated to 0.45 Gy (see Table 5 for sample details).

4.2 Relationship between OSL and TL

The TL measurements performed in this work served mainly to provide insight into the thermal and anomalous fading characteristics of the OSL signal. The TL curve of a resistor array irradiated to 2.5 Gy (generated as described in Section 3.3.2) is shown in Figure 24, along with 3-peak and 5-peak deconvolutions produced with the assistance of GlowFit (Puchalska and Bilski, 2006). The additional peaks clearly improve the fit (see the FOM in Table 6), particularly for the largest peak, where a single curve is unable to precisely match the observed peak shape at higher temperatures. The position of the largest peak, however, is similar for both fits (190°C for 3-peak, 184°C for 5-peak).

Table 6. FOM and maximum peak temperatures for 3-peak and 5-peak glow curve deconvolutions shown in Figure 26.

		3-peak fit	5-peak fit
	FOM (%)	12.9	9.8
T_{max} (°C)	Peak 1	93.2	94.4
	Peak 2	---	130.4
	Peak 3	189.8	184.1
	Peak 4	---	230.1
	Peak 5	332.0	320.5

As shown in Figure 25, the 190°C peak is photosensitive, and is almost completely depleted by 1000 seconds of stimulation with blue LEDs. The peak displays a significant shift upward in temperature with increasing illumination time.

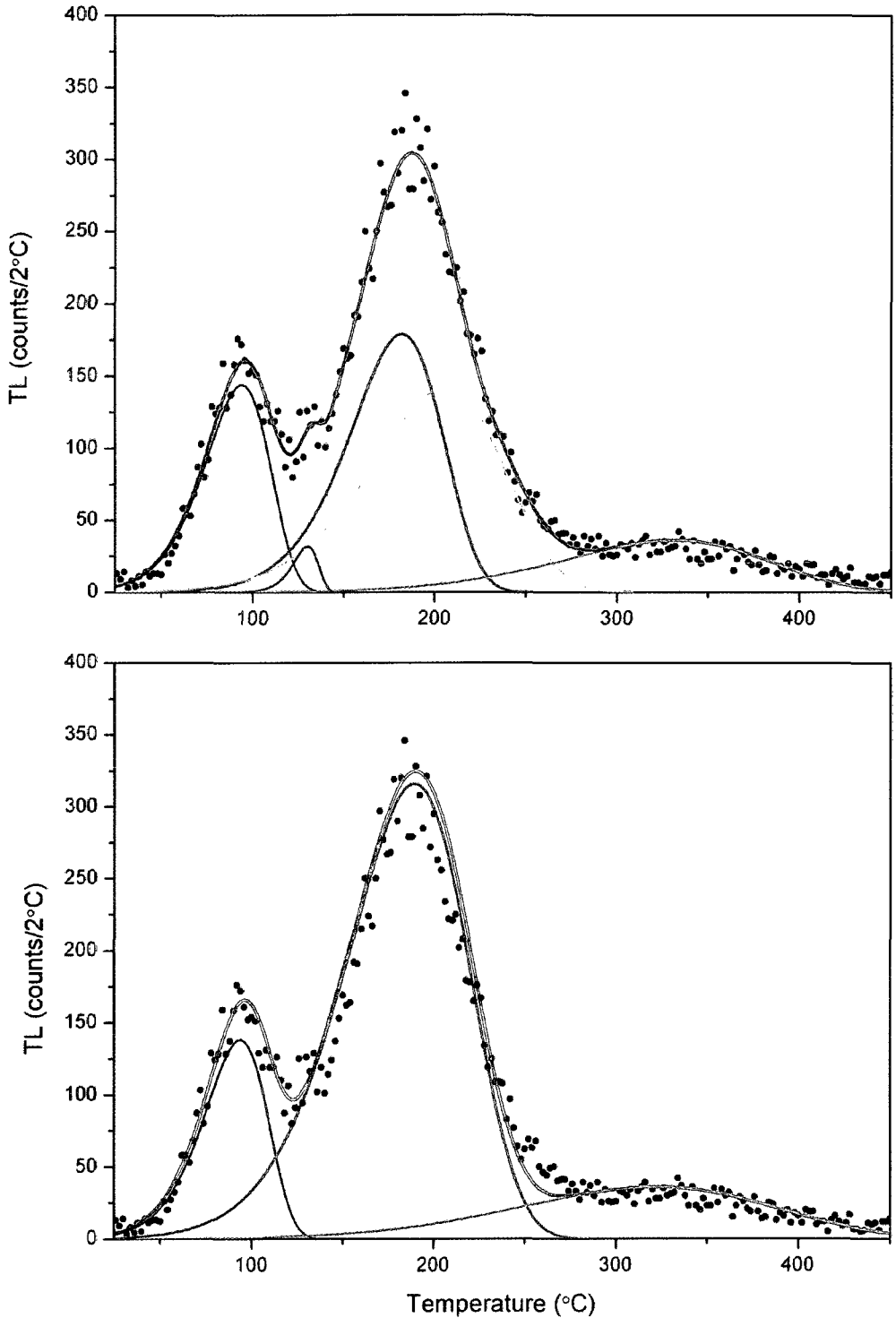

Figure 24. 5-peak (top) and 3-peak (bottom) deconvolutions of the TL glow curve of a 100Ω resistor array (Cal-Chip CN34J10CT) irradiated to 2.5 Gy.

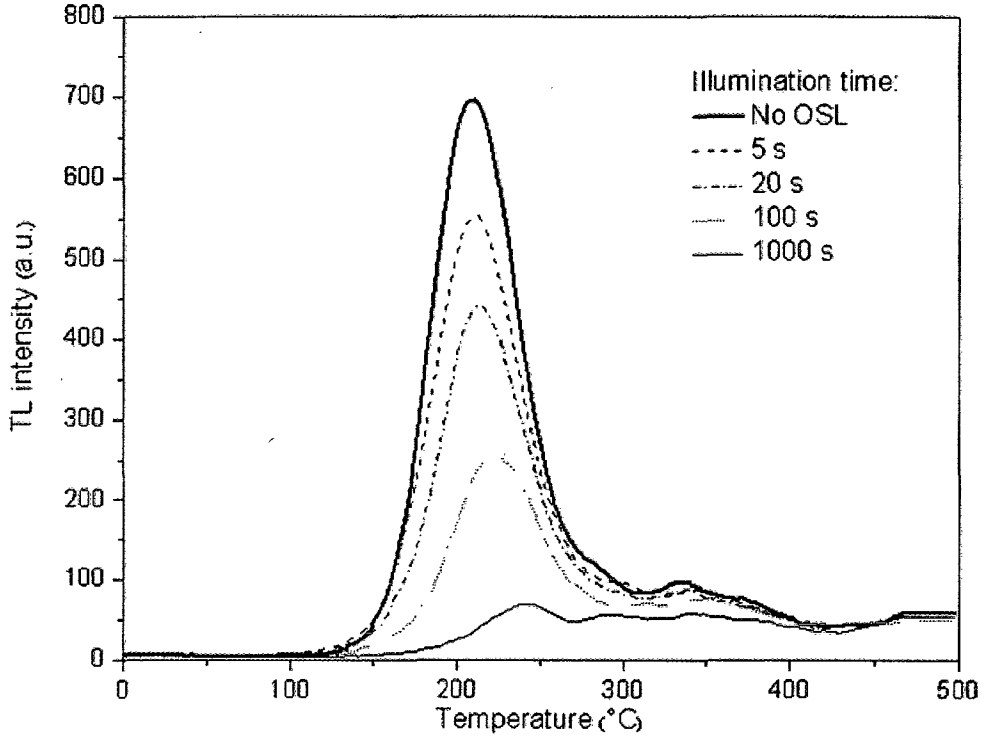

Figure 25. Depletion of TL signal by various durations of blue light stimulation for a set of six Cal-Chip 68.1 Ω resistors (RM10F68R1CT) irradiated to 2.1 Gy.

4.3 Determination of preheat and read temperatures

Based on the TL curve, which has a low-temperature peak centred at 93°C , a 10-second preheat to 120°C was considered sufficient to eliminate this thermally unstable portion of the signal without significantly depleting the 190°C TL peak.

Figure 26 shows how varying the sample temperature during OSL measurement affects the OSL emission from the sample. There is a gradual (but slight) increase in the net OSL up to a read temperature of 120°C , where it begins to decrease, most likely due to thermal quenching effects. An OSL read temperature of 90°C was selected, as it provides slightly improved luminescence efficiency without being so close to the 190°C TL peak as to cause thermal eviction from the trap(s) associated with this peak.

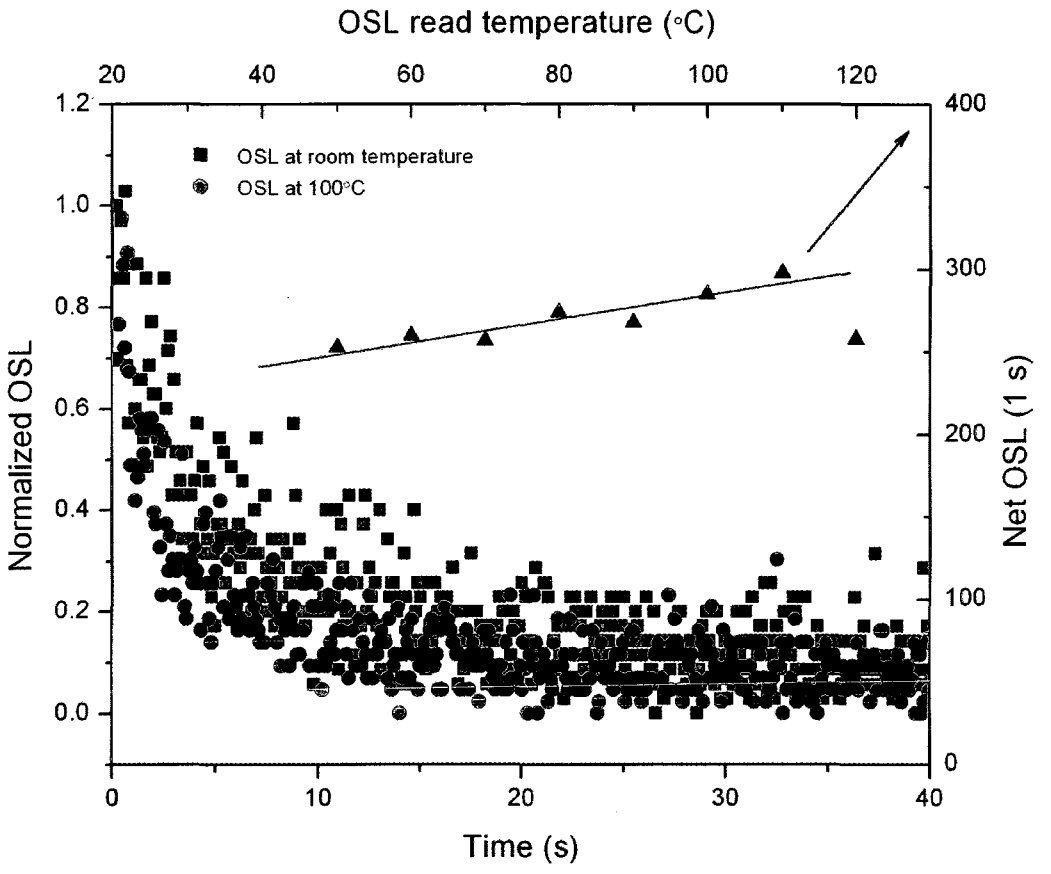

Figure 26. OSL curves and net OSL signal at various read temperatures for one Cal-Chip 68 Ω resistor (0.45 Gy, 130°C preheat).

4.4 Dose response curves and variability

Typical OSL curves from surface-mount resistors are shown below, in Figure 27. While a fast component clearly dominates the signal, being largely depleted in the first 10 s, there is a significant slow component; in fact, the signal does not fully return to background even following a 100 s illumination. The curves can be well modeled as a sum of exponential decays, but the parameters determined from such a fit are of little practical use in this application.

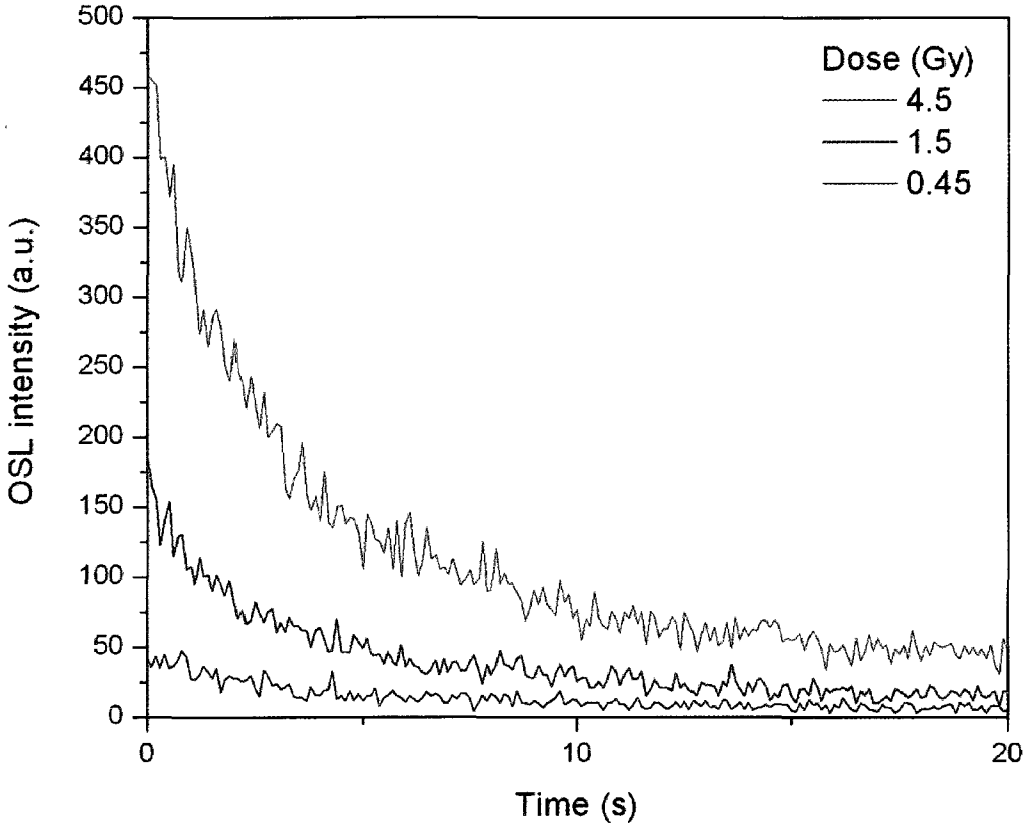

Figure 27. OSL response of a 73 mg sample of Cal-Chip 249 Ω surface-mount resistors (RM10F2490CT).

Figure 28 shows the linear dose response of a single Cal-Chip resistor over the range 0.32-107 Gy. Normalization to test doses was not done because there is very little change in sensitivity: the repeated point on the graph represents a 1 Gy dose given immediately following the 107 Gy measurement, and shows only a slight increase in sensitivity.

The response at lower doses (0.014 to 4.5 Gy) is shown in Figure 29, along with the one sigma limit of detection and 20% uncertainty level, determined as described in Section 3.3.1. For the set of 6 Cal-Chip resistors, it is estimated that a dose of under 0.04 Gy could be measured with 20% uncertainty.

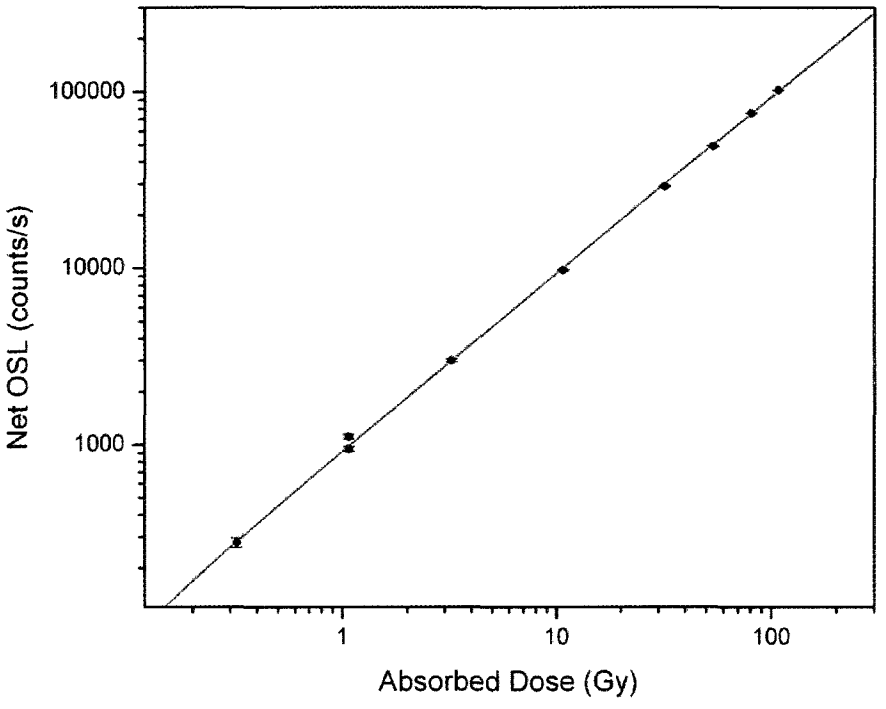

Figure 28. Dose response of one Cal-Chip 68.1 Ω surface-mount resistor (RM10F68R1CT) from 0.32 to 107 Gy

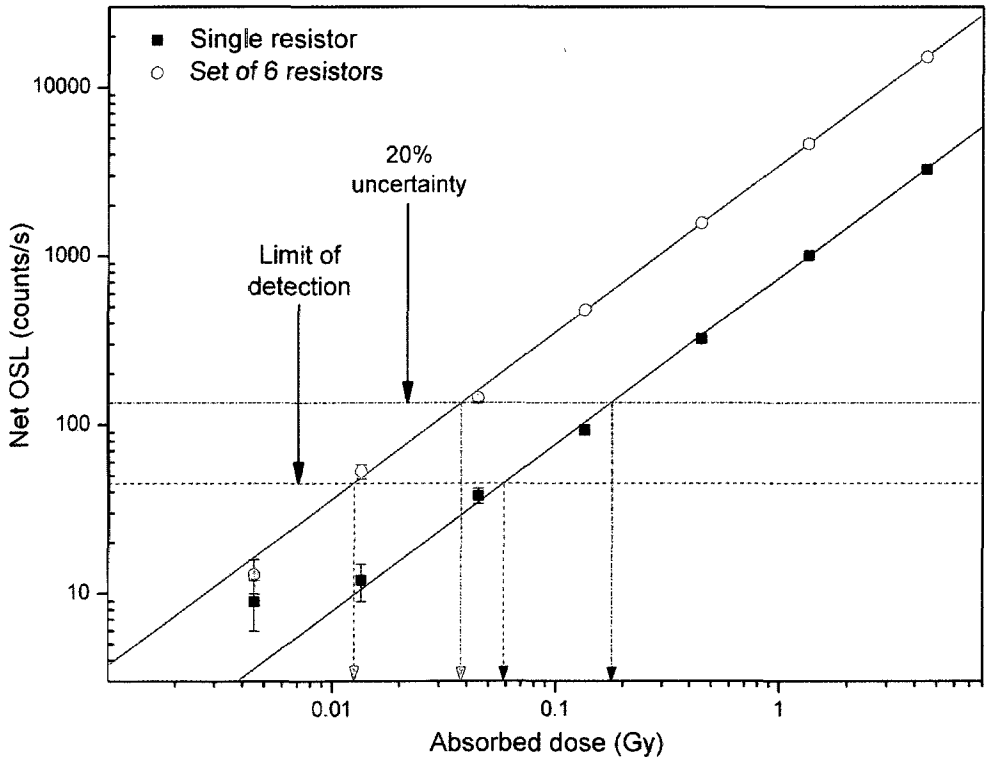

Figure 29. Dose response of Cal-Chip 68.1 Ω surface-mount resistors (RM10F68R1CT) from 0.014 to 4.5 Gy.

While the dose response sensitivities of the substrates varied widely between manufacturers and production lots, a minimum detectable dose on the order of 10 mGy was typical for an aliquot composed of several resistors. Figure 30 shows the variability of OSL response to a 0.45 Gy dose for different models of resistors of the same type (RM10 series) from the same supplier (Cal-Chip). The response from the most sensitive resistor was nearly six times that of the least sensitive, and the average response was 1555 counts, integrated over the first 3 seconds of the signal. It should be noted that the resistor exhibiting the lowest OSL response (68 Ω) is the identical model used to construct the dose response curves above.

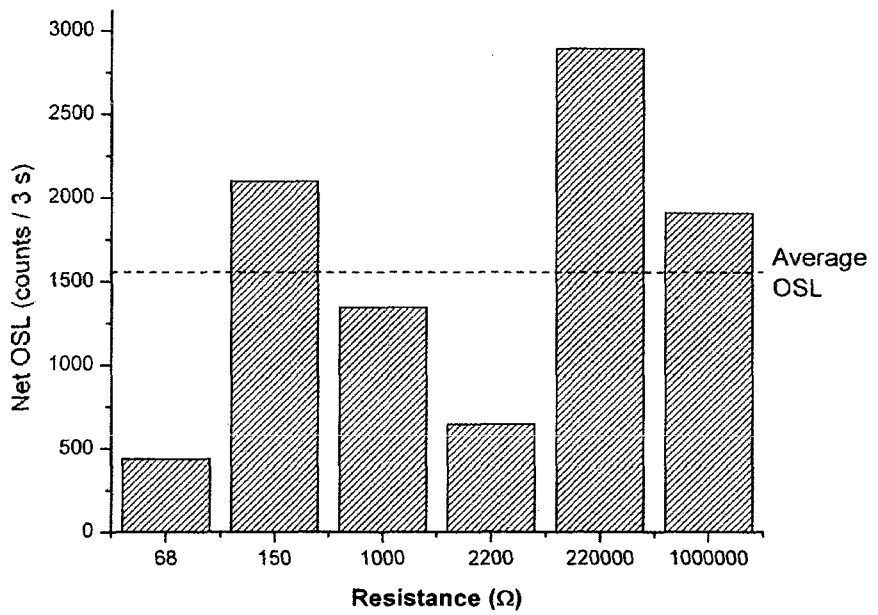

Figure 30. Average net OSL signal from various models of Cal-Chip RM10 series resistors irradiated to 0.45 Gy.

4.5 Discussion

The results of the early experiments described in this chapter led to the decision to focus all subsequent research on surface-mount resistors, which consistently emit OSL following irradiation, are easily identified, and appear in large numbers in all electronic devices. These

experiments also revealed some of the practical challenges of this kind of analysis. Take, for example, the blackening of the resistors (from electronic devices) described in Section 4.1. This observation led to the discovery that the epoxy adhesive used to secure the components to the circuit board (pictured in Figure 11) was interfering with the OSL emission from the ceramic substrate. In particular, once it had blackened following heating to elevated temperature, it blocked the OSL signal almost entirely. For this reason, the use of a solvent to remove as much of the adhesive as possible was incorporated into the analysis procedure described in Section 3.5, and high-temperature heating was eliminated.

4.5.1 TL and OSL characteristics

The TL and OSL curves, depicted in Figure 24 and Figure 27, show similar characteristics to those of Al_2O_3:C; the OSL curve shows a relatively slow decay, and the TL glow curve peaks, at approximately 93°C and 190°C, are similar to those observed in some "narrow peak" Al_2O_3:C samples (Akselrod and Akselrod, 2002). There are several reasons why the TL curve may be better fit with five peaks than three, despite the fact that there are only three obvious peaks. First, the deconvolution software (GlowFit) uses first-order kinetics to fit the TL peaks, so it is possible that the 190°C peak exhibits higher-order kinetics that are not well-modeled by the equations used in the software (Puchalska and Bilski, 2006). Woda *et al.* (2009) have recently done an in-depth study of the TL curves of alumina ceramics that suggests alternate explanations. A T_{Max}-T_{Stop} analysis (McKeever, 1985), used to resolve TL glow peaks, suggests the presence of a small 140°C TL peak, and the inclusion of this peak did indeed improve the fit of the curve. If this were the case, the use of a higher preheat temperature than the 120°C preheat used in these experiments would be warranted; in fact, even a 160°C preheat may prove

insufficient. In addition, Woda *et al.* (2009) suggest that the 190°C peak may not be a single peak, but may consist of several closely-spaced peaks or possibly a continuous distribution of peaks. This would help to explain the increase of T_{max} with increasing illumination time, observed in Figure 25 (depletion of TL following varying durations of OSL).

The optimal pre-heat temperature was selected solely on the basis of the temperatures of the peaks in the TL glow curve, with the goal of eliminating any thermally unstable signal. This is not really the best method of making such a determination; ideally, a preheat plateau test should be employed. This involves carrying out dose reconstruction using a SAR procedure with a range of different preheat temperatures. The dose calculated by this procedure is then plotted versus preheat temperature, and ideally this will identify a temperature range where the reconstructed dose is consistent, effectively a "plateau".

4.5.2 Dose response

The results of the dose response studies are encouraging. First, the OSL response is observed to increase linearly with dose over five orders of magnitude, meaning that doses can be reliably interpolated (or even extrapolated) from a dose response curve. The dose response curve constructed in Figure 29 suggests that low doses (less than 0.05 Gy) can be reconstructed with good accuracy; this is well below the level of concern for medical treatment for radiation exposure. The fact that the response of the 68 Ω resistors was less than one-third of the average response of the components compared in Figure 30 suggests that even lower detection limits may be achieved, depending on the quality of the sample.

It is important to note that, while properties such as sensitivity and fading rate have been observed to vary between resistors, the linearity of the dose response of aluminum oxide

substrates is consistent. Even though there is no prior knowledge of the dose response of a given sample (i.e. luminescence counts per Gy), regenerative dose methods allow this to be determined through the measurement of the OSL response of the sample to known doses, following the measurement of the OSL signal induced by the accident dose.

Unless otherwise specified, all of the doses reported in this work are doses in quartz, simply because quartz is used to calibrate the beta source in the automated OSL reader. In order to properly report dose in tissue, the energy response of the resistor substrates must be determined and the appropriate conversion factors calculated. Ultimately, the $^{90}Sr/^{90}Y$ source should be calibrated to a standard aluminum oxide ceramic material irradiated using a reference gamma-ray source.

CHAPTER 5:

RESULTS AND DISCUSSION – SIGNAL STABILITY AND FADING

Determination of signal stability is an important part of the characterization of any OSL-emitting material. When early experiments observed a loss of signal over time at room temperature, an in-depth study of this effect was undertaken. The aim was to determine how much of the signal loss was due to thermal fading, and how much, if any, could be attributed to anomalous fading behaviour. Figure 31 shows several TL curves from a surface-mount resistor sample. Following irradiation, the sample temperature is increased linearly at a rate of $5°C \cdot s^{-1}$, and the emitted luminescence is recorded. In this case, the TL curve is measured at various times following irradiation, with delays from 1.5 min to 8.4 h. As expected, the 93°C TL peak decays quickly at room temperature. What is surprising is the significant reduction in the 190°C TL peak, which should be fairly stable at room temperature, given that standard dosimetric materials such as TLD-500 have stable dosimetric peaks in this temperature range.

5.1 Automated short-term fading experiments

These experiments were carried out in two series, one for the three lowest preheat temperatures and a second for the three highest. Earlier experiments indicated that the sensitivity change of resistor substrates following repeated measurement cycles was negligible (Inrig *et al.*, 2008), and this was indeed the case for the lower-temperature preheats, so no sensitivity correction (through normalization to test doses) was applied. It was assumed that this would also be the case for the higher-temperature preheats; however, significant increases in sensitivity were observed for preheats of 200°C and 260°C, where the observed increases over the course of the measurement

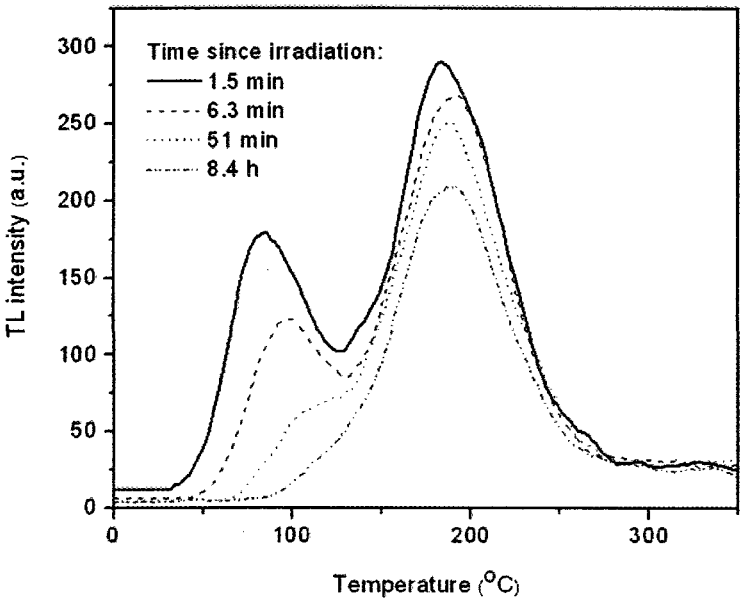

Figure 31. Anomalous fading of 190°C TL peak from 6 Cal-Chip 68.1 Ω resistors (RM10F68R1CT) irradiated to 2.2 Gy.

sequence were 7% and 21% respectively. Assuming a consistent sensitivity change over each cycle of irradiation and measurement, this is equivalent to a sensitivity increase of 0.5% per cycle for the 200°C preheat and 1.6% per cycle for the 260°C preheat. These values were used to correct each measurement for the incremental increase in sensitivity. In the case of the 160°C measurements, which were carried out after the sensitivity change was observed in the other measurements, a test dose was incorporated into the sequence in order to correct for any sensitivity change.

The results of short-term fading measurements carried out using preheat temperatures from 120°C to 260°C is shown in Figure 32. The fading curves are well-behaved, with a clear logarithmic dependence on the time since irradiation. The fading rate, g, is observed to decrease when the preheat temperature is increased, but fading is not eliminated, proving that anomalous fading is taking place. The observed fading rates varied from 15% per decade (120°C preheat) to 10.6% per decade (260°C preheat) for t_c = 8.3 h, calculated from the linear fit parameters according to Equation 18.

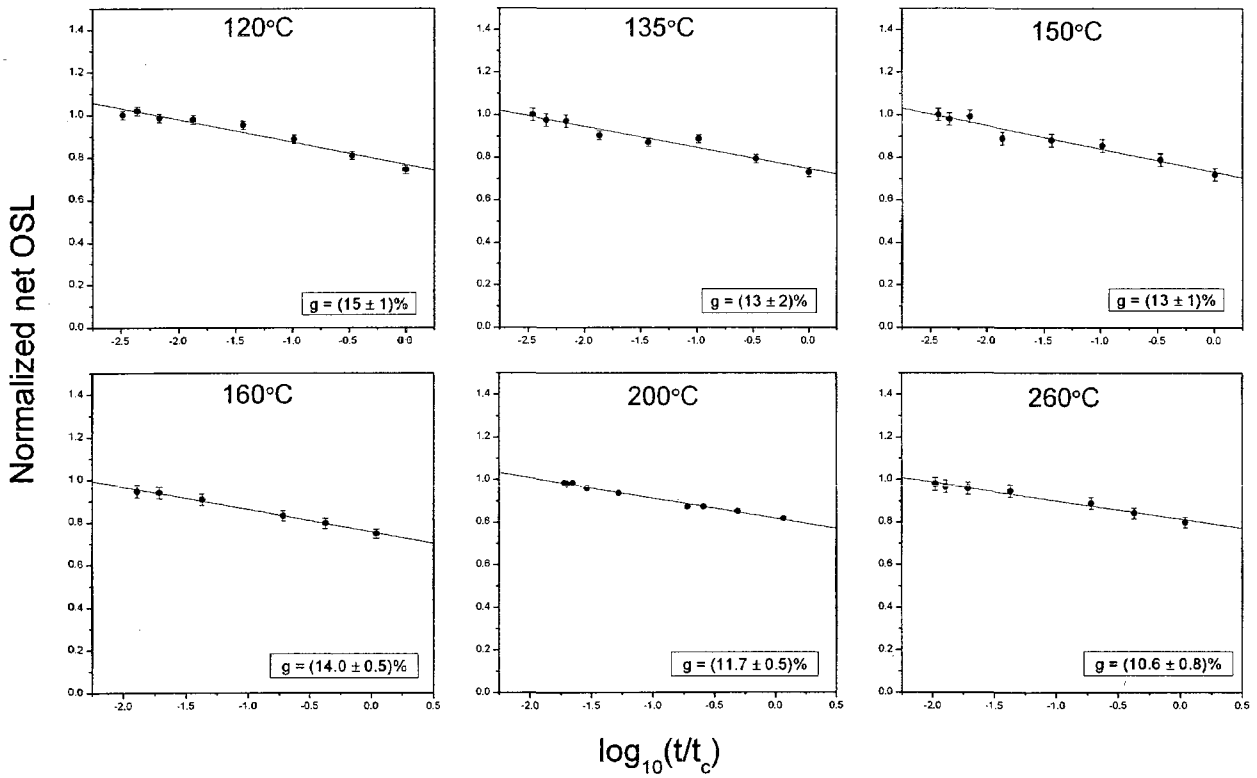

Figure 32. Variation of signal fading rate, g (in %/decade) with preheat temperature for t_c = 8.3 h.

The 120°C to 150°C plots show results for a single aliquot, resulting in fairly large uncertainties; in fact, there is no evidence for a statistically significant difference in fading rates using this range of preheat temperatures. The 160°C to 260°C plots, however, represent the average

fading behaviour of the 12 aliquots used in each experiment. Taking the average of the fit parameters for each aliquot calculated individually yields essentially the same result; however, there is significant sample-to-sample variation in the fading rate. Fading rates ranged from 9.4 – 18% for the 160°C preheat, 10.1 – 12.4% for the 200°C preheat, and 8.4 – 13% for the 260°C preheat.

While there appears to be a trend towards a lower fading rate with increased preheat temperature, this can only be deemed statistically significant for the 260°C preheat (relative to lower temperatures). Although the fading rate is slightly reduced in this case, the need to apply a fading correction is not eliminated.. In addition, the OSL signal (integrated over the first 1 s) following a 260°C preheat is lower by 77% relative to the signal following a 160°C preheat, as illustrated in Figure 33, below, presenting a clear disadvantage in terms of sensitivity.

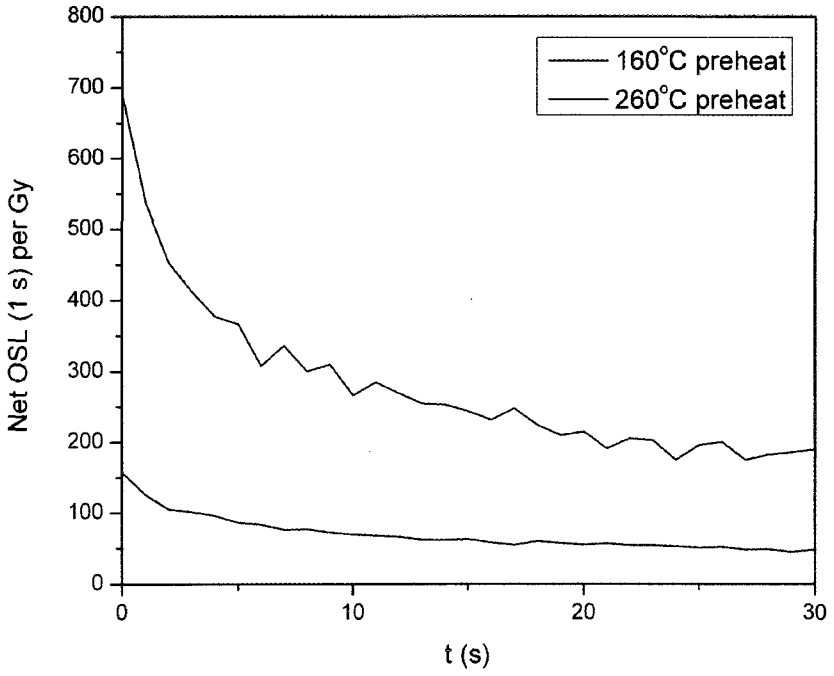

Figure 33. OSL signal following preheats to 160°C and 260°C

5.2 Long-term fading studies

The results of the first long-term fading study (using Cal-Chip resistor arrays) are shown in Figure 34. There is a fair degree of scatter in the results, but this can be attributed to the fact that each point on the graph represents a single OSL measurement on a sample consisting of a single resistor array. The advantage of thermal pre-treatment is clear; the signal from the unheated sample initially decays quite quickly before the signal begins to decrease linearly, approximately one day following irradiation. This is due to the fact that the unheated sample initially experiences both thermal and anomalous fading until all of the thermally unstable signal has decayed. By contrast, the signal from the preheated samples decreases linearly as a function of the logarithm of the time since irradiation. The value of g observed for the preheated samples is 17% per decade for t_c = 8.3 h, comparable to the 15% fading rate observed for the sample subjected to the same thermal treatment in the short-term study.

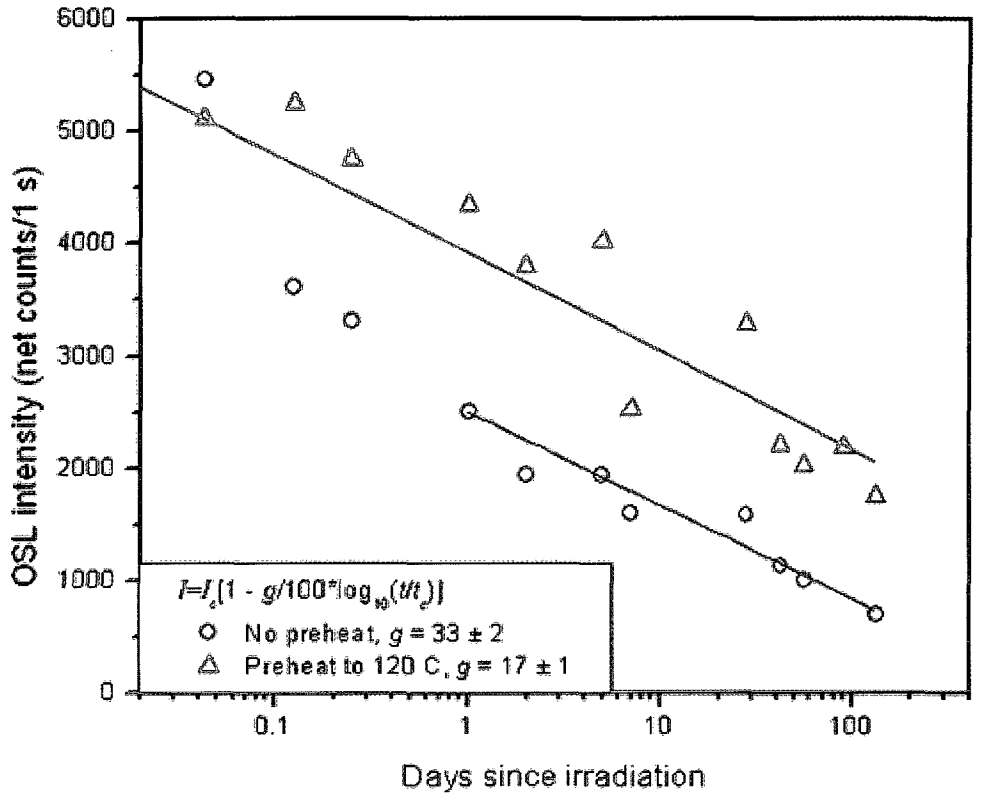

Figure 34. Long-term fading of OSL signal from Cal-Chip resistor arrays irradiated to 5 Gy with a ^{60}Co gamma source, with and without preheat.

The experiment was repeated with Bourns resistor samples in order to obtain more statistically sound results (10 resistors were used per sample) and to see if the fading rate varied significantly for resistors from another source. Figure 35 shows the results of the experiment, where the same type of logarithmic decay is observed. The calculated value of g, however, is significantly larger than that measured for the other resistors, at 24% per decade for the same value of t_c.

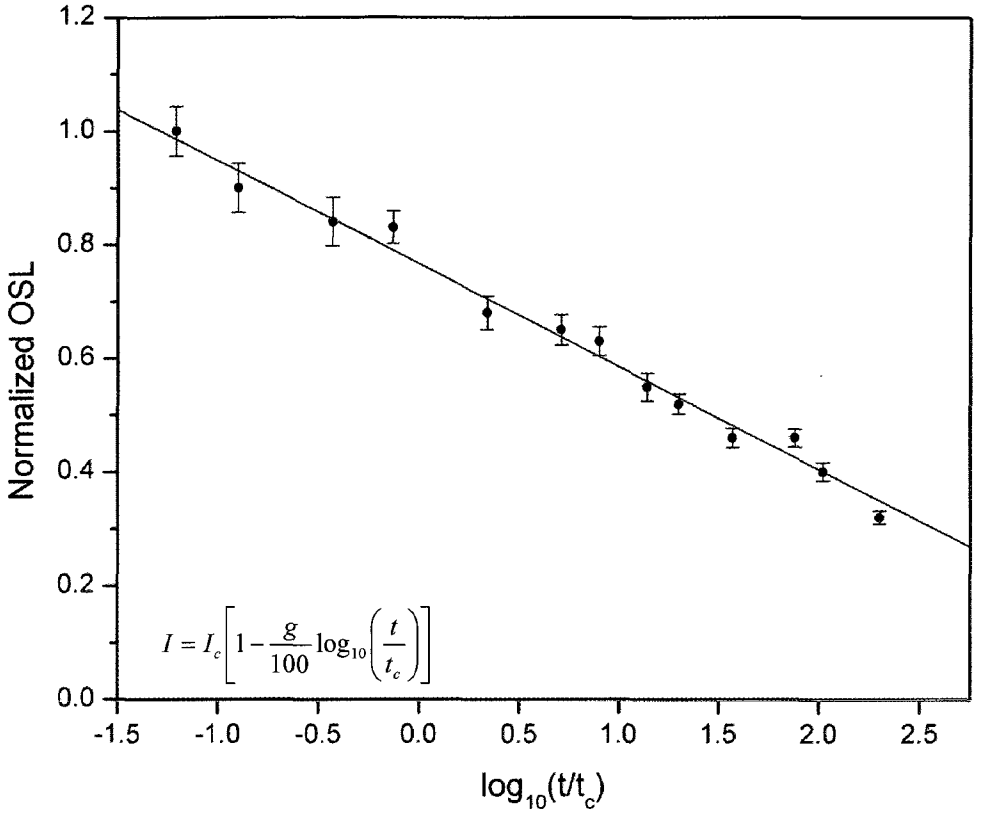

Figure 35. Anomalous fading of OSL signal from Bourns, Inc. resistor samples (CR0805-FX-1200E) irradiated to 5 Gy with a ^{60}Co gamma irradiator. The measured fading rate is 24 ± 1 %/decade for t_c = 0.346 d (8.3 h).

5.3 Discussion

5.3.1 The origin of OSL signal fading

It is difficult to determine whether any of the fading of the 190°C peak can be attributed to thermal eviction from the traps. Although the thermal half-life of a TL peak at a given temperature can be calculated from Equation 22, as discussed in Section 3.3.2, this is only effective if the fitting parameters truly reflect the physical model. Since the number of peaks used to fit the TL curve in Figure 24 was somewhat arbitrary, it seems unlikely that this is the case. In the case of TLD-100, Bos (2001) reported a factor of 24 discrepancy between the calculated and measured values of the thermal half-life of peak 2.

The observed signal instability raises a very interesting question: given the similarities between alumina porcelain (> 95% Al_2O_3) and Al_2O_3:C (TLD-500), why does the former exhibit anomalous fading while the latter does not? As discussed in Section 4.5, their OSL and TL curve shapes are very similar, with both having dosimetric peaks near 200°C. In addition, both display negligible sensitivity change over repeated cycles of heating and irradiation, allowing the use of a regenerative dose estimation procedure without sensitivity correction (see Section 2.5.2).

The best explanation for this discrepancy relies on the quantum-mechanical tunnelling model, in which the probability of a trapped electron escaping by tunnelling through a potential barrier is dependent on the optical excitation energy and the tunnelling distance to the recombination centre (Huntley and Lamothe, 2001). The lifetime is particularly dependent on the tunnelling distance; while a 5 nm distance between a trap and recombination centre may result in a lifetime of over a million years, a 3 nm spacing may reduce that lifetime to a few seconds (Aitken, 1985). If the defects are randomly distributed, there is a range of tunnelling distances, and correspondingly, a range of lifetimes. As a result, the closest trapped-electron recombination-centre pairs will tend to recombine first, with more distant pairs recombining as time elapses. This leads to the inverse dependence of the recombination rate on the time after irradiation. Integration of the recombination rateover time an expression for the number of trapped electrons remaining, resulting in the logarithmic dependence of the intensity of the OSL signal on the time after irradiation, as in Equation 18 (Huntley and Lamothe, 2001).

Al_2O_3:C is a standardized material, manufactured under strictly controlled conditions and engineered for optimal dosimetric properties, presumably resulting in a very regular lattice structure. By contrast, the alumina porcelain used in resistor substrates is used solely for its properties as a dielectric, and is manufactured to entirely different standards. It is likely that the

manufacturing process itself is primarily responsible for the observed fading behaviour. These substrates are likely fired to high temperatures and cooled rapidly. Rapid cooling would result in a less regular lattice structure, with a range of physical distances between electron traps and recombination centres, resulting in anomalous fading as described above.

5.3.2 Thermal treatment and signal fading

In the past, the wisdom of attempting to correct for fading in geological dating has been questioned, in part because it is impossible to verify whether fading rates observed in the laboratory are consistent over geological time scales (Aitken, 1985). In this case, however, the relatively short intervals between irradiation and analysis in a contemporary radiation event, plus the materials' remarkably stable cycle-to-cycle OSL sensitivity, allow for more accurate extrapolations of anomalous fading over the time scale of interest.

In terms of the effect of the preheat temperature on the fading rate, there is no apparent advantage to high thermal treatments, given that fading occurs regardless for the reasons discussed above. The lower the preheat employed, the greater the OSL signal intensity, and the lower the limit of detection. Even though doses below 0.5 Gy are of little immediate medical concern, it is desirable to have the lowest possible limit of detection, both for long-term studies of stochastic health effects and to reassure the worried-well that they are not in immediate danger. The sample-to-sample variability in measured fading rate was minimized by the 200°C preheat, while the 160°C preheat resulted in the greatest variation in fading rates. The possible existence of a TL peak at 140°C is discussed in Section 4.5, and the fading behaviour with 160°C may support this theory. Luminescence originating from a 140°C peak would not be completely eliminated by a 160°C preheat, likely resulting in greater fluctuations in OSL

measurements. Despite this, for maximum sensitivity, a preheat temperature of 160°C is tentatively recommended, pending the results of future preheat plateau experiments.

5.3.3 Fading corrections

These results suggest that, since the fading behaviour of the resistor it is indeed possible to apply a fading correction to ensure the accuracy of dose measurements, so long as the time since exposure can be approximated. What is not clear is whether it will be possible to apply a "universal" fading correction to obtain an initial dose estimate, or if there is so much variation between samples that the rate will need to be measured in each case. The former would be very desirable for the purposes of medical triage, where sample analysis must be done as quickly as possible; this is therefore an important subject for further study. The results of the short-term fading experiments, where large sample-to-sample variations in fading rate were observed, suggest that consistent fading behaviour cannot be assumed for resistors of the same type (even from the same lot), let alone of different types and origins. Nonetheless, this does not necessarily preclude the use of a universal fading correction, at least for the initial dose estimate, should the fading behaviour of resistor samples removed from devices (which will consist of many types of resistors of varying origins) prove to be reasonably consistent.

CHAPTER 6:

RESULTS AND DISCUSSION – SIMULATED RED TRIALS

6.1 Trial results

The results for one aliquot of resistors removed from a trial-irradiated cellular phone are shown in Figure 36, while results for all devices from both trials are summarized in Table 7. Because the samples exhibited a negligible OSL sensitivity change over the measurement sequence, normalization to the 43 mGy test dose did not change the dose estimates. It did, however increase their statistical noise; for this reason, the values in Table 7 are calculated from the net OSL signal without sensitivity correction. All dose estimates were within 0.02-0.15 Gy of the doses recorded by the MGP SOR/R electronic dosimeters (EDs), which (according to their specifications) are accurate to within 20%.

Table 7. Simulated RED trial results

	Device	Time after irradiation (days)	ED dose (Sv)	OSL dose (Gy)
Trial 1	Nokia 6160i	4.1	0.23 ± 0.05	0.28 ± 0.09
	Motorola 120c	9.1	0.30 ± 0.06	0.39 ± 0.11
	Nokia 3360	18.0	0.10 ± 0.02	0.10 ± 0.07
Trial 2	Nokia 6160i	20.9	0.27 ± 0.05	0.42 ± 0.14
	Motorola 120c	20.9	0.57 ± 0.11	0.78 ± 0.21
	Nokia 3360	20.9	0.09 ± 0.02	0.08 ± 0.04
	Blackberry	20.9	0.10 ± 0.02	0.16 ± 0.06

The fading-corrected signal, shown in Figure 36, was calculated from Equation 22 using the value of g determined from the second series of long-term fading experiments (i.e., 24% per decade) as these results were the most statistically robust of the long-term fading studies.

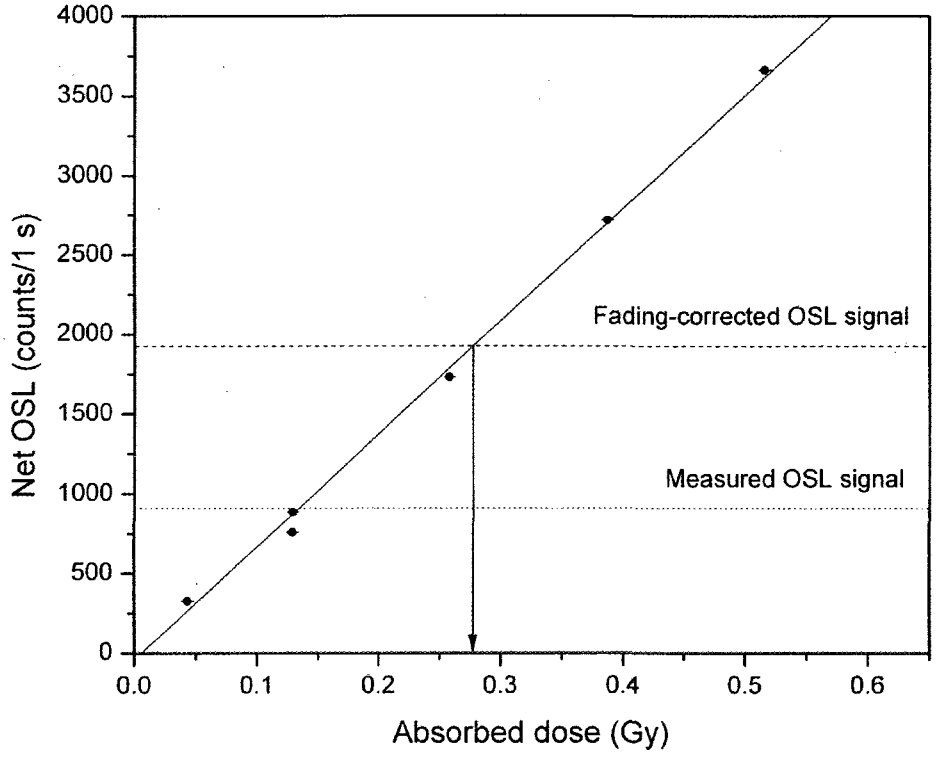

Figure 36. Dose reconstruction for Nokia 6160i (Trial 1). Because the sensitivity change between cycles was found to be negligible, regeneration doses were not normalized to test doses.

6.2 Discussion

6.2.1 Dose reconstruction

These trials were intended to reproduce, with some degree of realism, a chain of events that might lead to a requirement for individual dose reconstruction. All of the procedures described in the previous chapters were employed in order to arrive at an estimate of the accident dose. Since many of the cellular devices used in the trials were analysed at different times following irradiation, the validity of the fading correction could be tested. It should be pointed out that the

dose estimates produced by this method are estimates of external dose only. In the case of purely external exposures (such as would result from an RED or exposure to an orphaned source), this is sufficient, but in the case of an RDD or nuclear detonation, this estimate would only represent one component of the total radiation dose.

There are a great many sources of uncertainty, some due to the nature of the trial, and others introduced by the analysis methods. Many of the devices were placed quite close to the ^{137}Cs source, so various parts of the same device may have received significantly different doses, and even though the EDs and devices were in close proximity to one another, they would likely have received a dose different from the average dose to the resistors. The value of g used for the fading correcting was only an estimate, and it is difficult to say at this stage how well it reflects average fading behaviour, although the relatively good agreement of the corrected doses with the ED doses suggests it is in the right range.

6.2.2 Proposed improvements to procedures

The process of extracting components from electronic devices, removing the residual adhesive, and preparing samples for analysis is still difficult and time-consuming, particularly as it must be done under darkroom conditions. Another approach, such as crushing the extracted resistors before analysis, is worth considering. This would have several advantages: there would be a greater amount of material available for analysis (as previously only the surface of the component could emit OSL), the tedious task of placing miniscule components substrate-up on planchettes would be eliminated, and the removal of adhesives using solvents might no longer be required. Before this method can be recommended, experiments must be carried out in order to determine whether or not crushing affects the OSL signal, as mechanical forces are known to induce triboluminescence in some materials.

6.2.3 Future work

It would be valuable to repeat this type of analysis several times, with entire devices irradiated to known doses using a gamma irradiator (such as the GB-150C). The doses in these trials were quite small, and the effectiveness of the analysis method over a larger range of doses should be studied. Another issue that should be explored is the effect of operation of a cellular phone on the OSL signal from its components. Depending on the temperature reached within the resistors, it is possible that some of the signal may be depleted. It is important to determine to what extent that may be the case, since victims in a mass-casualty scenario will unquestionably be using cellular phones and other communications devices immediately after an event.

CHAPTER 7: SUMMARY AND CONCLUSIONS

This work has demonstrated the potential for the use of components of cellular phones and similar devices as "fortuitous" dosimeters following a radiological accident or terrorist event. The primary focus has been the characterization of the alumina ceramic substrates of surface-mount resistors found in all such devices. To that end, the dose response of these substrates was studied, revealing a linear OSL response to doses over a range of five orders of magnitude, with minimal sensitivity change. Unlike Al_2O_3:C, alumina ceramics have been shown to demonstrate anomalous fading that is essentially independent of thermal treatment. Short-term and long-term fading experiments revealed that it is possible to correct for this fading, with the caveat that the potential for a "universal" fading model is unknown as of yet. Fading rates ranging from 10 – 25% per decade (a tenfold increase in the time after irradiation) were observed.

Trials designed to simulate an individual's exposure to a radiological exposure device (RED) successfully reconstructed doses of less than 0.1 Gy at times ranging from 4 days to 3 weeks following exposure. That being said, the success of these trials is regarded as proof of this OSL analysis technique in principle only. Before dose estimates arrived at in this way can be considered reliable, a great deal of work remains to be done.

With further development, this fortuitous dosimetry technique will provide a new and extremely valuable tool for rapid post-event dose assessment. Future work will include additional studies to measure the variability of anomalous fading rates, to determine the effect of device operation following irradiation on the OSL signal of the components, and to explore, and ideally improve, the upper and lower detection limits of this technique.

REFERENCES

ADAMIEC, G., STONEHAM, D. & GÖKSU, Y. (1997) Accident dose estimation using porcelain. A comparison between different thermoluminescence methods. *Radiation Measurements,* 27, 389-392.

AITKEN, M. J. (1985) *Thermoluminescence Dating,* Orlando, Academic Press.

AITKEN, M. J. (1998) *An Introduction to Optical Dating,* Oxford, Oxford University Press.

AKSELROD, M. S. & KORTOV, V. S. (1990) Thermoluminescent and Exoemission Properties of New High-Sensitivity TLD-Al 2 O 3: C Crystals. *Radiation Protection Dosimetry,* 33, 123-126.

AKSELROD, M. S., KORTOV, V. S., KRAVETSKY, D. J. & GOTLIB, V. I. (1990) Highly Sensitive Thermoluminescent Anion-Defective Alpha-Al203:C Single Crystal Detectors. *Radiation Protection Dosimetry,* 32, 15-20.

AKSELROD, M. S. & MCKEEVER, S. W. S. (1999) A Radiation Dosimetry Method Using Pulsed Optically Stimulated Luminescence. *Radiation Protection Dosimetry,* 81, 167-175.

ANTONOV-ROMANOVSKII, V. V., KEIRUM-MARCUS, I. F., POROSHINA, M. S. & TRAPEZNIKOVA, Z. A. (1955) *Conference of the Academy of Sciences of the USSR on the Peaceful Uses of Atomic Energy.* Moscow.

BAILEY, R. M., ADAMIEC, G. & RHODES, E. J. (2000) OSL properties of NaCl relative to dating and dosimetry. *Radiation Measurements,* 32, 717-723.

BAILIFF, I. K. (1995) The use of ceramics for retrospective dosimetry in the Chernobyl exclusion zone. *Radiation Measurements,* 24, 507-511.

BAILIFF, I. K. & POOLTON, N. R. J. (1991) Studies of charge transfer mechanisms in feldspars. *Nuclear Tracks and Radiation Measurements,* 18, 111-118.

BAILIFF, I. K. & STEPANENKO, V. (1996) Final Report, ECP 10: Retrospective dosimetry and dose reconstruction. IN BAILIFF, I. K. & STEPANENKO, V. (Eds.), European Commission.

BANERJEE, D., BØTTER-JENSEN, L. & MURRAY, A. S. (2000) Retrospective dosimetry: Estimation of the dose to quartz using the single-aliquot regenerative-dose protocol. *Applied Radiation and Isotopes,* 52, 831-844.

BEERTEN, K., WODA, C. & VANHAVERE, F. (2009) Thermoluminescence dosimetry of electronic components from personal objects. *Radiation Measurements,* In Press, Corrected Proof.

BORTOLOT, V. J. (1997) Improved OSL excitation with fiberoptics and focused lamps. *Radiation Measurements,* 27, 101-106.

BORTOLOT, V. J. (2000) A new modular high capacity OSL reader system. *Radiation Measurements,* 32, 751-757.

BOS, A. J. J. (2001) High sensitivity thermoluminescence dosimetry. Nuclear Instruments and Methods in Physics Research, Section B: Beam Interactions with Materials and Atoms, 184, 3-28.

BØTTER-JENSEN, L. (1997) Luminescence techniques: instrumentation and methods. *Radiation Measurements,* 27, 749-768.

BØTTER-JENSEN, L. (2000) Development of Optically Stimulated Luminescence Techniques using Natural Minerals and Ceramics, and their Application to Retrospective Dosimetry. Copenhagen, University of Copenhagen.

BØTTER-JENSEN, L., ANDERSEN, C. E., DULLER, G. A. T. & MURRAY, A. S. (2003a) Developments in radiation, stimulation and observation facilities in luminescence measurements. *Radiation Measurements,* 37, 535-541.

BØTTER-JENSEN, L., BANERJEE, D., JUNGNER, H. & MURRAY, A. S. (1999) Retrospective Assessment of Environmental Dose Rates Using Optically Stimulated Luminescence from Al2O3:C and Quartz. *Radiation Protection Dosimetry,* 84, 537-542.

BØTTER-JENSEN, L., BULUR, E., DULLER, G. A. T. & MURRAY, A. S. (2000) Advances in luminescence instrument systems. *Radiation Measurements,* 32, 523-528.

BØTTER-JENSEN, L. & DULLER, G. A. T. (1992) A new system for measuring optically stimulated luminescence from quartz samples. *International Journal of Radiation Applications and Instrumentation. Part D. Nuclear Tracks and Radiation Measurements* 20, 549-553.

BØTTER-JENSEN, L., JUNGNER, H. & POOLTON, N. R. J. (1995) A continuous OSL scanning method for analysis of radiation depth-dose profiles in bricks. *Radiation Measurements,* 24, 525-529.

BØTTER-JENSEN, L. & MCKEEVER, S. W. S. (1996) Optically Stimulated Luminescence Dosimetry Using Natural and Synthetic Materials. *Radiation Protection Dosimetry,* 65, 273-280.

BØTTER-JENSEN, L., MCKEEVER, S. W. S. & WINTLE, A. G. (2003b) *Optically Stimulated Luminescence Dosimetry*, Elsevier.

BRÄUNLICH, P., SHAFER, D. & SHARMANN, A. (1965) A Simple Model for Thermoluminescence and Thermally Stimulated Conductivity of Inorganic Photoconducting Phosphors and Experiments Pertaining to Infrared-stimulated Luminescence. *1st Int. Conf. on Luminescence Dosimetry.* Stanford.

BRAY, H. E., BAILEY, R. M. & STOKES, S. (2002) Quantification of cross-irradiation and cross-illumination using a Riso TL/OSL DA-15 reader. *Radiation Measurements,* 35, 275-280.

CAL-CHIP ELECTRONICS (2007) Ingredient Table of the Chip Resistor - RM06 Series. Ivyland, PA.

CHEN, R. & LEUNG, P. L. (2003) The decay of OSL signals as stretched-exponential functions. *Radiation Measurements,* 37, 519-526.

CHEN, R. & MCKEEVER, S. W. S. (1997) *Theory of Thermoluminescence and Related Phenomena*, World Scientific.

CHOUGAONKAR, M. P. & BHATT, B. C. (2004) Blue light stimulated luminescence in calcium fluoride, its characteristics and implications in radiation dosimetry. *Radiation Protection Dosimetry,* 112, 311-321.

CURIE, M. (1903) Recherches sur les substances radioactives. Paris, Gauthiers-Villars.

DULLER, G. A. T. (1991) Equivalent dose determination using single aliquots. International journal of radiation applications and instrumentation. Part D. Nuclear tracks and measurements, 18, 371-378.

DULLER, G. A. T. & BØTTER-JENSEN, L. (1993) Luminescence from Potassium Feldspars Stimulated by Infrared and Green Light. *Radiation Protection Dosimetry,* 47, 683-688.

GALLOWAY, R. B. (1996) Equivalent dose determination using only one sample: alternative analysis of data obtained from infrared stimulation of feldspars. *Radiation Measurements,* 26, 103-106.

GODFREY-SMITH, D. I. (2006) Applicability of moissanite, a monocrystalline form of silicon carbide,to retrospective and forensic dosimetry. *Radiation Measurements,* 41, 976-981.

GODFREY-SMITH, D. I. & HASKELL, E. H. (1993) Application of optically stimulated luminescence to the dosimetry of recent radiation events involving low total absorbed doses. *Health Physics,* 65, 396-404.

GÖKSU, H. Y. (2003) Telephone chip-cards as individual dosemeters. *Radiation Measurements,* 37, 617-620.

GÖKSU, H. Y. & BAILIFF, I. K. (2006) Luminescence dosimetry using building materials and personal objects. *Radiation Protection Dosimetry,* 119, 413-420.

GÖKSU, H. Y., BAILIFF, I. K. & MIKHAILIK, V. B. (2003) New approaches to retrospective dosimetry using cementitious building materials. *Radiation Measurements,* 37, 323-327.

HUNTLEY, D. J., GODFREY-SMITH, D. I. & THEWALT, M. L. W. (1985) Optical dating of sediments. *Nature,* 313, 105-107.

HUNTLEY, D. J. & LAMOTHE, M. (2001) Ubiquity of anomalous fading in K-feldspars and the measurement and correction for it in optical dating. *Canadian Journal of Earth Sciences,* 38, 1093-1106.

HUNTLEY, D. J., SHORT, M. A. & DUNPHY, K. (1996) Deep traps in quartz and their use for optical dating. *Canadian Journal of Physics,* 74, 81-91.

IAEA (1998) Planning the Medical Response to Radiological Accidents. *IAEA Safety Reports Series No. 4.* Vienna, International Atomic Energy Agency.

INRIG, E. L., GODFREY-SMITH, D. I. & KHANNA, S. (2008) Optically stimulated luminescence of electronic components for forensic, retrospective, and accident dosimetry. *Radiation Measurements,* 43, 726-730.

JUNGNER, H. & BØTTER-JENSEN, L. (1994) Study of sensitivity change of OSL signals from quartz and feldspars as a function of preheat temperature. *Radiation Measurements,* 23, 621-624.

LAMOTHE, M. & AUCLAIR, M. (1999) A solution to anomalous fading and age shortfalls in optical dating of feldspar minerals. *Earth and Planetary Science Letters,* 171, 319-323.

LAMOTHE, M. & AUCLAIR, M. (2000) The fadia method: a new approach in luminescence dating using the analysis of single feldspar grains. *Radiation Measurements,* 32, 433-438.

LARSSON, C., KOSLOWSKY, V., GAO, H., KHANNA, S. & ESTAN, D. (2005) Optically stimulated luminescence in forensics. *Applied Radiation and Isotopes,* 63, 689-695.

LI, S. H. & YIN, G. M. (2006) Luminescence properties of biotite relevant to dating and dosimetry. *Journal of Luminescence,* 121, 51-56.

MARKEY, B. G., BÃ˜TTER-JENSEN, L. & DULLER, G. A. T. (1997) A new flexible system for measuring thermally and optically stimulated luminescence. *Radiation Measurements,* 27, 83-89.

MATHUR, V. K., BARKYOUMB, J. H., YUKIHARA, E. G. & GÖKSU, H. Y. (2007) Radiation sensitivity of memory chip module of an ID card. *Radiation Measurements,* 42, 43-48.

MCKEEVER, S. W. S. (1985) *Thermoluminescence of Solids*, Cambridge University Press.

MCKEEVER, S. W. S. (2002) New Millennium Frontiers of Luminescence Dosimetry. *Radiation Protection Dosimetry,* 100, 27-32.

MCKEEVER, S. W. S., AKSELROD, M. S. & MARKEY, B. G. (1996a) Pulsed Optically Stimulated Luminescence Dosimetry Using Alpha-Al2O3:C. *Radiation Protection Dosimetry,* 65, 267-272.

MCKEEVER, S. W. S., BØTTER-JENSEN, L., AGERSNAP LARSEN, N., MEJDAHL, V. & POOLTON, N. R. J. (1996b) Optically Stimulated Luminescence Sensitivity Changes in Quartz Due to Repeated Use in Single Aliquot Readout: Experiments and Computer Simulations. *Radiation Protection Dosimetry,* 65, 49-54.

MCKEEVER, S. W. S., BØTTER-JENSEN, L., LARSEN, N. A. & DULLER, G. A. T. (1997a) Temperature dependence of OSL decay curves: experimental and theoretical aspects. *Radiation Measurements,* 27, 161-170.

MCKEEVER, S. W. S., LARSEN, N. A., BØTTER-JENSEN, L. & MEJDAHL, V. (1997b) OSL sensitivity changes during single aliquot procedures: computer simulations. *Radiation Measurements,* 27, 75-82.

MCKINLAY, A. F. (1981) *Thermoluminescence Dosimetry*, Adam Hilger.

MOSCOVITCH, M., TAWIL, R. A. & SVINKIN, M. (1993) Light Induced Fading in Alpha-Al2O3:C. *Radiation Protection Dosimetry,* 47, 251-253.

MURRAY, A. S. & MEJDAHL, V. (1999) Comparison of regenerative-dose single-aliquot and multiple-aliquot (SARA) protocols using heated quartz from archaeological sites. *Quaternary Geochronology,* 18, 223-229.

MURRAY, A. S. & ROBERTS, R. G. (1998) Measurement of the equivalent dose in quartz using a regenerative-dose single-aliquot protocol. *Radiation Measurements,* 29, 503-515.

MURRAY, A. S., ROBERTS, R. G. & WINTLE, A. G. (1997) Equivalent dose measurement using a single aliquot of quartz. *Radiation Measurements,* 27, 171-184.

MURRAY, A. S. & WINTLE, A. G. (2000) Luminescence dating of quartz using an improved single-aliquot regenerative-dose protocol. *Radiation Measurements,* 32, 57-73.

NIEDERMAYER, B, M., GÖKSU, A, H. Y., DALHEIMER, B, A., BAYER & B, A. (2000) Infrared (IR) stimulated luminescence from modern bricks in retrospective dosimetry applications. *Radiation Measurements,* 32, 825-832.

PRADHAN, A. S., LEE, J.I., KIM, J.L. (2008) Recent developments of optically stimulated luminescence materials and techniques for radiation dosimetry and clinical applications. *Journal of Medical Physics,* 33.

PUCHALSKA, M. & BILSKI, P. (2006) GlowFit-a new tool for thermoluminescence glow-curve deconvolution. *Radiation Measurements,* 41, 659-664.

RISØ DTU (2008) Guide to "The Risø TL/OSL Reader". Denmark, Risø DTU.

SANBORN, E. N. & BEARD, E. L. (1965) Sulfides of Strontium, Calcium and Magnesium in Infrared-stimulated Luminescence Dosimetry. *1st Int. Conf. on Luminescence Dosimetry.* Stanford.

SMITH, B. W., RHODES, E. J., STOKES, S. & SPOONER, N. A. (1990) The Optical Dating of Sediments Using Quartz. *Radiation Protection Dosimetry,* 34, 75-78.

STONEHAM, D. (1984) The use of porcelain to assess gamma ray doses. *Hiroshima/Nagasaki Dose Reassessment Workshop.* University of Utah, Radiobiology Division.

THOMSEN, K. J., BØTTER-JENSEN, L. & S. MURRAY, A. (2002) Household and Workplace Chemicals as Retrospective Luminescence Dosemeters. *Radiation Protection Dosimetry,* 101, 515-518.

U.S. DEPARTMENT OF HOMELAND SECURITY (2005) Technology Assessment and Roadmap for the Emergency Radiation Dose Assessment Program (ERDAP). Homeland Security Science and Technology, UCRL-TR-215887.

VISOCEKAS, R. (1985) Tunnelling radiative recombination in labradorite: its association with anomalous fading of thermoluminescence. *Nuclear tracks and radiation measurements,* 10, 521-529.

WINTLE, A. G. (1973) Anomalous fading of thermoluminescence in mineral samples. *Nature,* 245, 143-144.

WODA, C., GREILICH, S., BEERTEN, K. (2009) On the OSL curve shape and preheat treatment of electronic components from portable electronic devices. *Radiation Measurements,* In Press.

APPENDIX: SAMPLE CALCULATIONS

A.1 Derivation of fading correction equations

The approach used here is taken from Huntley and Lamothe (2001). For convenience, calculations are done using the natural logarithm form of the fading equation:

$$I(t) = I(t_c)\left(1 - \kappa \ln\frac{t}{t_c}\right) \tag{A.1}$$

Variables are defined as follows:

t'	Time since start of irradiation
T	Duration of irradiation
I_0	Intensity resulting from irradiation for time T *without fading*
T_L	Laboratory storage time (i.e. time between end of irradiation and OSL measurement)

The fading equation follows from integrating the expression for the phosphorescence (afterglow) intensity,

$$-\frac{dI}{dt} \propto \frac{1}{t}$$

The intensity at measurement time due to the irradiation over time interval dt' is therefore

$$dI = \frac{I_0}{T} dt' \left[1 - \kappa \ln\left(\frac{T + T_L - t'}{t_c}\right)\right]$$

Integration yields the total intensity at measurement time:

$$I = \frac{I_0}{T}\int_0^T \left(1 - \kappa \ln\left(\frac{T + T_L - t'}{t_c}\right)\right) dt'$$

Evaluating over the irradiation period,

$$I = \frac{I_0}{T}\left[t' + \kappa t_c\left(\left(\frac{T+T_L-t'}{t_c}\right)\ln\left(\frac{T+T_L-t'}{t_c}\right)+\frac{t'}{t_c}\right)\right]_0^T$$

$$I = I_0\left\{(1+\kappa)+\kappa\left[\frac{T_L}{T\ln\left(\frac{T_L}{t_c}\right)}-\left(1+\frac{T_L}{T}\right)\ln\left(\frac{T+T_L}{t_c}\right)\right]\right\} \quad \text{(A.2)}$$

A.2 Calculation of fading correction factors

For convenience, the data shown in Figure 35 (anomalous fading of Bourns Inc. resistors) is re-plotted with a natural logarithm scale and with t_c set to the time of the first measurement (~0.5 h). Huntley and Lamothe (2001) suggest that t_c be taken as the time between laboratory irradiation and measurement; that is, the pause before measurement of the regeneration doses. The issue here is that laboratory measurements were taken with only a brief delay between irradiation and measurement (i.e. minutes), and the fading equations are not well-behaved as $t \to 0$. Instead, the ratio between the signal at the time of laboratory measurement, t_m, (approximately 90 s following irradiation) and t_c is calculated from Figure 37 as R_c = 1.22 ± 0.04. $I(t)$ / $I(t_c)$ is then calculated from Equation A.2, in the case of Trial 1, where the duration of the irradiation is not negligible relative to the time between irradiation and measurement, or Equation A.1, in the case of Trial 2.

The fading correction factors (summarized in Table 8) are calculated as follows,

$$f = \frac{I(t)}{I(t_c)}\frac{I(t_c)}{I(t_m)} = \frac{I(t_c)}{R_c I(t)}$$

and the fading-corrected OSL signal will thus be given by $OSL_f = OSL / f$.

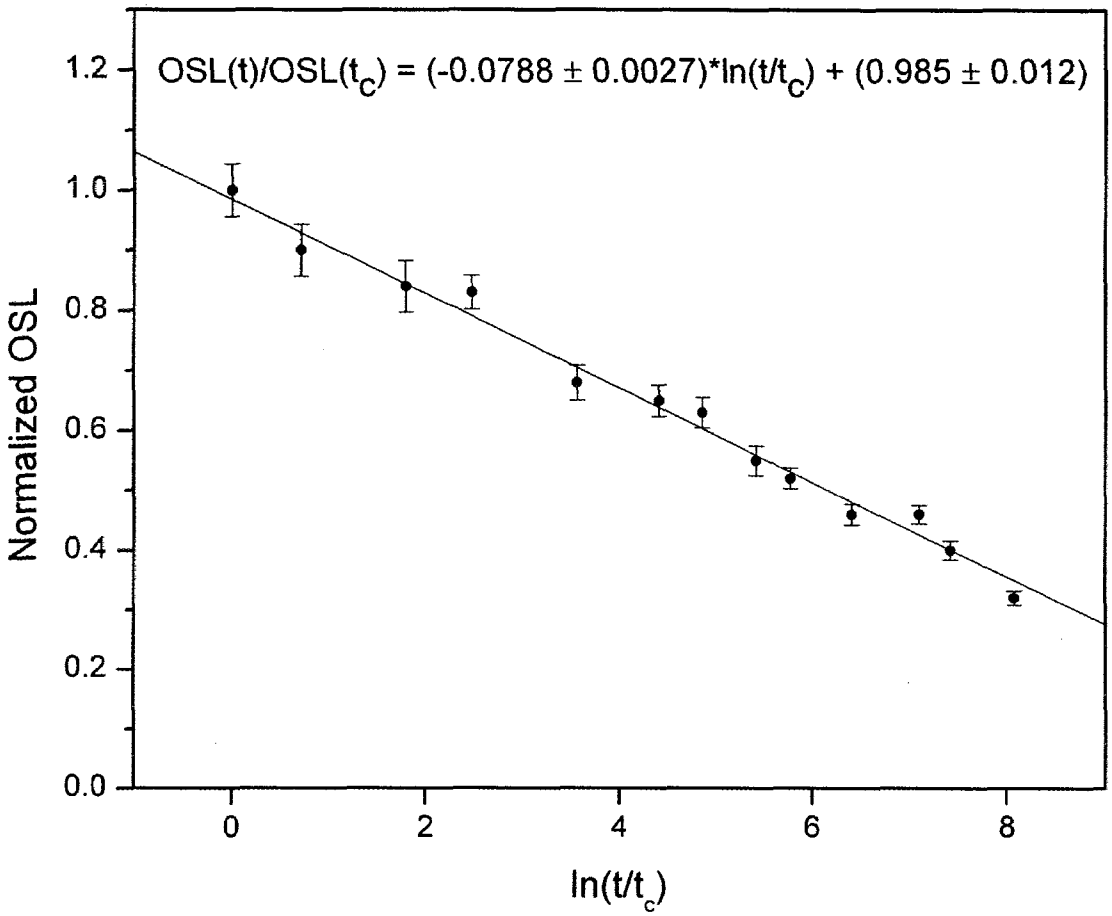

Figure 37. Anomalous fading of Bourns Inc. resistors for fading corrections.

Table 8. Fading correction factors

	Device(s)	Time after irradiation (days)	Fading correction factor
Trial 1	Nokia 6160i	4.1	0.47 ± 0.13
	Motorola 120c	9.1	0.42 ± 0.15
	Nokia 3360	18.0	0.38 ± 0.16
Trial 2	All	20.9	0.37 ± 0.16

A.3 Calculation of OSL dose

Dose response data for the Nokia 6160i cellular phone analysed in Trial 1 are summarized in Table 9. The net OSL as a function of dose was plotted as in Figure 36, and a linear regression was performed, yielding the following dose response equation:

$$OSL = mD + b$$

where D is the dose (calibrated to dose in quartz, in Gy), and m and b are the slope and intercept of the dose response curve, respectively. Rearranging gives

$$D = \frac{OSL - b}{m}$$

Table 9. Dose response data for Nokia 6160i (Trial 1)

Irradiation time (s)	Gross OSL		Dose (Gy)	Net 1 s OSL	Relative uncertainty
	Ch. 1-10	Ch. 951-1000			
–	957	234	Unknown	910	0.03
10	350	105	0.043	329	0.06
30	794	176	0.129	759	0.04
30	924	194	0.129	885	0.04
60	1785	269	0.258	1731	0.02
90	2791	356	0.387	2720	0.02
120	3762	500	0.516	3662	0.02

The linear regression gives $m = 7171 \pm 182$ and $b = -67 \pm 43$.

Taking into account fading, the dose estimate and associated uncertainty are given by

$$D = \frac{\frac{OSL}{f} - b}{m}$$

$$\Delta D = \sqrt{(\Delta m)^2\left(\frac{\partial D}{\partial m}\right)^2 + (\Delta b)^2\left(\frac{\partial D}{\partial b}\right)^2 + (\Delta f)^2\left(\frac{\partial D}{\partial f}\right)^2 + (\Delta OSL)^2\left(\frac{\partial D}{\partial OSL}\right)^2}$$

$$\Delta D = \sqrt{\left(\frac{\Delta m\left(b - \frac{OSL}{f}\right)}{m^2}\right)^2 + \left(-\frac{\Delta b}{m}\right)^2 + \left(-\frac{\Delta f \cdot OSL}{f^2 m}\right)^2 + \left(\frac{\Delta OSL}{fm}\right)^2}$$

This gives D = 0.28 ± 0.07 Gy. Additionally, taking into consideration the uncertainty on the dose rate calibration, estimated at 5%, D = 0.28 ± 0.09.